UQAC
UNIVERSITÉ DU QUÉBEC
À CHICOUTIMI

Impact of mechanical site preparation on soil carbon in boreal lichen woodlands in Quebec

Par Karan Kumar Singh

Mémoire présenté à l'Université du Québec à Chicoutimi en vue de l'obtention du grade de Maîtrise ès sciences (M. Sc.) en ressources renouvelables

Québec, Canada

RÉSUMÉ

Les forêts boréales représentent l'un des plus grands réservoirs de carbone terrestres de la planète. Au sein de ce biome, les landes à lichens (LL) sont des écosystèmes ouverts et peu productifs qui se développent naturellement à la suite de perturbations successives. En raison de leur faible couvert arboré, les LL ont été identifiées comme d'excellentes candidates pour le boisement afin de séquestrer le carbone atmosphérique et atténuer les changements climatiques. Cependant, le succès de l'établissement des semis dans ces environnements hostiles nécessite un travail du sol (i.e., scarifiage) intensif. Bien que le scarifiage améliore la croissance initiale des arbres en créant des sillons minéraux et des monticules organiques, il perturbe gravement le sol forestier. La mesure dans laquelle cette perturbation déstabilise les réservoirs de carbone du sol existants et crée une « dette de carbone » demeure une incertitude critique dans les modèles de budget de carbone.

Ce mémoire de maîtrise a examiné les impacts à court et moyen termes du scarifiage sur la dynamique et la stabilité du carbone organique du sol et le cycle des nutriments dans les LL boréales. En utilisant une approche par chronoséquence dans la région du Saguenay–Lac-Saint-Jean, au Québec (Canada), nous avons comparé une portion de sol non-perturbée (intersillon) à des portions de sols perturbées (sillons et monticules) dans deux sites de la région du Saguenay–Lac-Saint-Jean ayant été scarifiés 4 ans (2020) et 12 ans (2012) avant l'échantillonnage. Nous avons quantifié les stocks de carbone totaux et évalué la vulnérabilité de la matière organique du sol (MOS) par fractionnement physique (matière organique particulaire [MOP] par rapport à la matière organique associée aux minéraux [MOAM]) et par des incubations en laboratoire mesurant la respiration basale et la sensibilité à la température (Q_{10}).

Nos résultats suggèrent que l'impact du scarifiage sur le carbone du sol est étroitement lié au temps écoulé depuis le travail du sol, bien que l'influence potentielle des variations inhérentes aux sites ne puisse être totalement exclue en raison de la nature non répliquée de la chronoséquence. Alors que les stocks de carbone sont restés stables 4 ans après la perturbation, le site scarifié il y a 12 ans a affiché une perte nette et sévère de carbone de 7,2 à 9,1 t C ha^{-1} dans l'horizon organique. Cette apparente dette de carbone à l'échelle de l'écosystème serait attribuable à une perte de végétation et probablement à l'interruption des apports de litière qui en découle, ainsi qu'à une perte de carbone par minéralisation microbienne de la MOP. De plus, bien que le brassage physique des monticules organiques avec le sol minéral lors du scarifiage réduise considérablement la concentration en carbone, la perte réelle de stock semble être d'origine biologique et surviendrait après un temps de latence de la décomposition. Le fractionnement du sol a révélé que, bien que le sol minéral soit dominé par une MOAM plus ancienne et fortement transformée, sa texture naturellement sableuse limite sa capacité à agir comme puits de carbone pour compenser les pertes de l'horizon organique.

Au final, cette recherche souligne que le scarifiage intensif dans les LL semble déclencher une dette de carbone importante et différée dans le temps. Néanmoins, nos résultats suggèrent qu'une partie du carbone des monticules est possiblement transférée vers le sol minéral sous forme de carbone organique dissous. Ainsi, les pertes nettes de carbone pourraient être plus faibles que celles mesurées dans cette étude. Une caractérisation plus précise de ces flux devra être faite. En conclusion, les futurs modèles de comptabilisation du carbone et les stratégies sylvicoles devront explicitement tenir compte de la vulnérabilité de la fraction MOP, de l'influence de l'hétérogénéité spatiale, et de l'épuisement progressif du réservoir de carbone du sol à la suite d'une perturbation physique afin d'évaluer avec précision le véritable potentiel d'atténuation climatique du boisement boréal.

Mots-clés: scarifiage, carbone organique du sol, landes à lichens, dette carbone, fractionnement de la matière organique.

ABSTRACT

Boreal forests represent one of the largest terrestrial carbon reservoirs on the planet. Within this biome, lichen woodlands (LWs) are open-canopy, low-productivity ecosystems that naturally arise following successive disturbances. Because of their sparse tree cover, LWs have been identified as prime candidates for afforestation to sequester atmospheric carbon and mitigate climate change. However, successful seedling establishment in these harsh environments requires intensive mechanical site preparation (MSP), such as scarification. While MSP improves early tree growth by creating mineral furrows and organic mounds, it severely disrupts the forest floor. The extent to which this disturbance destabilizes existing soil carbon pools and creates a "carbon debt" remains a critical uncertainty in global carbon budget models.

This study investigated the long-term impacts of MSP on soil organic carbon dynamics, stability, and nutrient cycling in boreal LWs. Utilizing a chronosequence approach in the Saguenay–Lac-Saint-Jean region of Québec, Canada, we compared an undisturbed control environment against two afforested sites scarified 4 years (2020) and 12 years (2012) prior to sampling. We quantified total carbon stocks and assessed soil organic matter (SOM) vulnerability through physical fractionation (Particulate vs. Mineral-Associated Organic Matter; POM and MAOM) and laboratory incubations measuring basal respiration and temperature sensitivity (Q_{10}).

Our findings suggest that the impact of MSP on soil carbon is closely linked to the time elapsed since disturbance, though inherent site-level variations cannot be entirely ruled out due to the unreplicated nature of the chronosequence. While carbon stocks remained stable 4 years post-disturbance, a net carbon loss of 7.2–9.1 t C ha^{-1} from the organic horizon was found 12 years after MSP. This ecosystem-level carbon debt is likely driven by the loss of plant biomass, the subsequent lack of litter input from this vegetation, the severing of fresh carbon inputs from the vegetation and the subsequent, unbuffered microbial mineralization of the physically unprotected POM fraction. Furthermore, while the physical dilution of the organic mounds with mineral layer during scarification drastically reduces carbon concentration, the actual C stock loss is biologically driven following an initial decomposition lag. Soil fractionation revealed that the organic horizons are overwhelmingly dominated by POM with a higher C:N ratio than MAOM, confirming the inherent vulnerability of this largely undecomposed carbon pool once the physical structure of the forest floor is disrupted.

Ultimately, this research highlights that intensive scarification in LWs causes a significant, time-delayed carbon debt, whose magnitude seems to be site-dependent. Additionally, observed dissolved organic carbon (DOC) dynamics suggest a potential downward migration of soluble carbon from the disturbed organic layer into the underlying mineral layer. To accurately evaluate the true climate mitigation potential of boreal afforestation, future carbon accounting models and silvicultural strategies must explicitly account for the vulnerability of the POM

fraction, the influence of spatial heterogeneity and the progressive exhaustion of the soil carbon pool following physical disturbance.

Keywords: Mechanical site preparation (MSP), Soil carbon dynamics, Lichen woodlands, Carbon debt, Soil organic matter fractionation.

Table of Contents

LIST OF FIGURES

LIST OF TABLES

ACKNOWLEDGEMENTS

I would like to express my sincere gratitude to my supervisor, Dr. Patrick Faubert, and my co-supervisors, Dr. Charles Marty and Dr. Maxime Paré, for their invaluable guidance, support, and encouragement throughout my master's research. Their expertise, insight, and mentorship have been instrumental in shaping both the direction and the quality of this work. I am deeply appreciative of their constructive feedback, thoughtful discussions, and continued support, all of which have greatly enriched this project and my development as a researcher. Furthermore, I would like to extend my special thanks to Julien Walter and his team for their invaluable technical advice and assistance regarding the experimental setup for measuring dissolved organic carbon (DOC).

I would also like to extend my appreciation to the entire Carbone boréal team, whose collaboration and support made this research possible. I am especially grateful to Carbone boréal for their financial support during my master's studies, which enabled me to conduct fieldwork and data analysis with the necessary resources and independence.

This study was also funded by the Ministère des Ressources naturelles et des Forêts (MRNF) of Québec (by the Contrat de service de recherche forestière number 3323-2326-REX-2206-74 obtained by Maxime Paré and Patrick Faubert). Carbone boréal gratefully acknowledges the in-kind contributions from the MRNF and the Ministère de l'Agriculture, des Pêcheries et de l'Alimentation of Québec.

To my colleagues and friends in the laboratory, thank you for fostering a supportive and intellectually stimulating environment that made each step of this journey both meaningful and enjoyable. Finally, I am deeply thankful to my family, and friends for their unwavering encouragement and support. Whether near or far, they have been a constant source of strength and motivation throughout this journey.

AVANT-PROPOS

Ce mémoire est structuré sous la forme d'un article scientifique. Les sections se déclinent comme suit : Chapitre 1 – Introduction générale, Chapitre 2 – l'article scientifique (avec ses sections), Chapitre 3 – Conclusion générale. L'article scientifique du chapitre 2 sera soumis à *Geoderma*. Les auteurs de l'article seront Karan Kumar Singh et les membres de sa direction de recherche (Charles Marty, Patrick Faubert et Maxime Paré).

CHAPTER I

GENERAL INTRODUCTION

The boreal forest represents one of the world's largest terrestrial carbon reservoirs, playing a pivotal role in the global climate system through both biophysical and biochemical processes. Globally, terrestrial ecosystems store approximately 3,550 Gt C, distributed across vegetation (450 Gt C), soils (1,700 Gt C), and permafrost (1,400 Gt C) (Friedlingstein et al., 2026). While forests cover only about 30–35% of the Earth's surface, they contain a disproportionately large share of these stocks, sequestering approximately 861 Gt C (Pan et al., 2011). Within this reservoir, the boreal forest alone accounts for nearly 30% of global forest carbon stocks, holding roughly 272 Gt C (Pan et al., 2011). In Quebec, the boreal landscape is not a homogenous closed-canopy forest but rather a mosaic that includes Boreal Lichen Woodlands (LWs) ecosystems characterized by sparse tree cover and low soil productivity, often resulting from successive natural disturbances like wildfires (Bernier et al., 2011). Distinguished by their specific vegetation structure, LWs possess a dense ground cover of terricolous lichens, primarily *Cladonia* species (e.g., *Cladonia stellaris*, *C. rangiferina*), interspersed with ericaceous shrubs such as *Rhododendron groenlandicum* and *Kalmia angustifolia* (Nilsson & Wardle, 2005; Payette & Delwaide, 2018). These ecosystems play a vital role in carbon storage and biodiversity support (Bradshaw et al., 2009; Girard et al., 2009). However, the ecological significance of LWs extends beyond their carbon storage capacity; they serve as critical habitats for various species and contribute to the overall health of the forest ecosystem (Payette & Delwaide, 2018).

To mitigate climate change, large-scale afforestation and reforestation initiatives are increasingly being prioritized as essential nature-based solutions (NBS) (Faubert et al., 2023; IPCC, 2022). Within this framework, the Carbone boréal initiative, led by the Université du Québec à Chicoutimi (UQAC), seeks to afforest these open LWs to enhance atmospheric CO_2 sequestration (Faubert et al., 2023). However, the transition from an open LW to a managed forest involves significant ecological trade-offs. The biochemical stability of soil organic carbon (SOC) following high-intensity management practices remains a critical area of scientific inquiry (Marty et al., 2024).

Figure 1: The field view of scarified boreal lichen woodlands (left panel; Photo by Carbone boréal) and the scarifier (right panel; Photo by the Resolute Forest Products blog).

To ensure the success of afforestation of LWs, Mechanical Site Preparation (MSP) is a standard forestry practice (Marty et al., 2024). MSP techniques such as scarification, physically alter the forest floor to expose mineral layer, creating mounds (M), furrows (F) and Inter-Furrow (IF) (Figure 1). While this process is proven to enhance tree survival and growth by improving seedling access to soil nutrients (Munson et al., 1993; Thiffault et al., 2013) and heat (Örlander et al., 1990;

Prévost, 1992), MSP simultaneously disturbs the stability of the soil structure. The disturbance of the humus layer and the exposure of mineral layer may trigger significant carbon fluxes. Current literature suggests that while MSP promotes above-ground biomass growth (Boateng et al., 2006; Lafleur et al., 2011), it may inadvertently stimulate the mineralization of centuries-old soil carbon, potentially offsetting the gain of carbon measured through plant growth (Jandl et al., 2007).

Despite the widespread use of MSP in Quebec's boreal regions, there is a significant knowledge gap regarding its impact on soil carbon stocks and dynamics in LWs. Previous research has identified a reduction in carbon concentration in the humus layer of disturbed areas, suggesting that carbon is lost from surface layers through both enhanced microbial respiration and downward migration of carbon into mineral horizons (Marty et al., 2024). However, the fate of this carbon – whether it is lost to the atmosphere as CO_2 or leached into deeper mineral horizons as dissolved organic carbon (DOC) – remains unquantified.

To accurately predict these potential atmospheric losses, it is crucial to understand the temperature sensitivity of soil organic matter (SOM) decomposition, typically expressed as the Q_{10} value. Fundamentally, the Q_{10} coefficient is a broad thermodynamic metric used to quantify the temperature dependence of various chemical reaction rates and biological processes (Mundim et al., 2020). In the specific context of soil ecology, the Q_{10} metric represents the factor by which the microbial respiration rate increases with every 10°C rise in temperature. This value is a fundamental parameter in carbon cycling models, yet the Q_{10} of organic carbon mineralization in these disturbed compartments (M and F) compared to undisturbed

IF is poorly documented. This is a critical omission for regional modeling; for instance, the Carbon Budget Model of the Canadian Forest Sector (CBM-CFS3), used to calculate carbon budgets at the stand scale, employs a Q_{10} of 2.65 for aboveground dead organic matter (DOM) and 2.0 for belowground DOM (Kull, 2019). Because these values are applied broadly, they remain highly uncertain and may not be adequate for the unique climatic conditions of boreal LWs following scarification.

Beyond carbon dynamics, it is equally essential to understand how MSP influences soil nutrient availability, particularly nitrogen. In the boreal forest, nitrogen is the most limiting element (LeBauer & Treseder, 2008; Schulte-Uebbing & de Vries, 2018). Its availability partially controls tree growth and, by extension, the strength of the aboveground carbon reservoir. MSP alters the physical soil environment, which can subsequently shift the rates of microbial nitrogen mineralization. Without a precise understanding of how MSP influences both soil carbon stability and the release of limiting nutrients such as nitrogen, predicting the "net climate benefit" of afforestation in LWs remains an estimation rather than a scientific certainty.

The primary goal of this research is to evaluate the effects of MSP on soil carbon dynamics in the LWs of the Saguenay-Lac-Saint-Jean region. Specifically, this study aims to quantify SOC and nitrogen stocks across different compartments (M, F, and IF) to estimate the net loss of these elements following MSP, and to analyze the stability, mineralization rate, and temperature sensitivity (Q_{10}) of SOC, nitrogen, and phosphorus through controlled soil incubations at varying temperatures, and to assess the flux of Dissolved Organic Carbon (DOC) through soil horizons to

distinguish between potential carbon translocation from top disturbed organic layers to underneath mineral layer and atmospheric loss. Collectively, these analyses will help fill the knowledge gap regarding how MSP alters soil carbon dynamics and indicators such as organic matter fractionation under different temperature conditions (Sutinen et al., 2019).

This research is driven by environmental, economic, and political imperatives. Environmentally, it contributes to the fundamental understanding of soil health in boreal ecosystems. Politically and economically, as carbon offsetting markets become increasingly central to climate policy, the accuracy of carbon sequestration data is paramount. By providing evidence on the biochemical impacts of MSP, specifically how physical disturbance alters the long-term stability of SOM and subsequent nutrient availability. This study offers insights into the broader carbon dynamics of LWs. While representing a focused scale of two sites, these insights provide essential data on impact of MSP. Ultimately, this detailed understanding can inform broader modeling efforts and future regional assessments, contributing to the goal of ensuring that afforestation programs in Quebec yield genuine carbon sequestratio

CHAPTER II

Impact of mechanical site preparation on soil carbon in boreal lichen woodlands in Quebec

Authors: Karan Kumar Singh[1,2,3,*], Charles Marty[1,3], Patrick Faubert[1,2,3], Maxime Paré[1,2,3]

Affiliations:
[1]Carbone boréal, Département des sciences fondamentales, Université du Québec à Chicoutimi, Saguenay, Canada;
[2]Laboratoire sur les écosystèmes terrestres boréaux (EcoTer), Département des sciences fondamentales, Université du Québec à Chicoutimi, Saguenay, Canada;
[3]Centre de recherche sur la boréalie (CREB), Université du Québec à Chicoutimi, Saguenay, Canada;

*Corresponding author: kksingh1@etu.uqac.ca

Note:

This chapter is presented as a scientific article. The article is planned to be submitted to *Geoderma*.

2.1 Abstract

Mechanical site preparation (MSP) creates furrows of exposed mineral layer and mounds of displaced organic layer to enhance forest regeneration, yet its long-term effects on soil carbon dynamics remain poorly understood. In boreal lichen woodlands (LWs; open-canopy ecosystems characterized by low productivity and slow organic matter turnover), understanding how MSP influences soil carbon content, composition, and stability is crucial for accurately estimating the "carbon loss" associated with afforestation.

This study investigated the temporal effects of MSP in two LWs located in Saguenay–Lac-Saint-Jean, Québec, Canada, scarified in 2012 and 2020. Soil samples were collected from mounds (M), furrows (F), and undisturbed inter-furrows (IF). We evaluated carbon stocks and the stability of SOM through physical fractionation of Particulate Organic Matter (POM) vs. Mineral-Associated Organic Matter (MAOM) and laboratory incubations at 15°C, 22°C, and 30°C to assess basal respiration and temperature sensitivity (Q_{10}).

Our results suggest an apparent time-dependent response to MSP, though the potential influence of inherent site-level differences cannot be entirely ruled out due to the unreplicated nature of the chronosequence. At the recently disturbed 2020 site, carbon stocks and concentrations remained stable. However, at the site scarified in 2012, carbon concentration in the organic M declined significantly from 32.5% (undisturbed IF) to 17.8%. While this concentration drop is largely a physical artifact resulting from dilution by mineral layer mixing during scarification, our mass-budget analysis estimated a net ecosystem loss of 7.2 to 9.1 t C ha^{-1} from the organic

horizon after 12 years. Fractionation revealed a stark horizon dichotomy largely unaffected by MSP: organic horizons were dominated by POM (85-95%), while mineral layer were dominated by MAOM (60-80%). The MAOM fraction exhibited consistently lower C:N ratios (10-20) compared to the physically unprotected POM (20-35), confirming that MAOM is composed of older, more heavily decomposed organic matter. Laboratory incubations showed that undisturbed IF organic horizons exhibited significantly higher basal respiration rates than the 12-year-old mounds ($P = 0.007$). This suggests that the disturbance of the soil structure and the destruction of the plant biomass cause the displaced mounds to progressively exhaust their finite labile carbon pool, leading to mid-term substrate limitation. Furthermore, nitrogen (NH_4) and phosphorus (PO_4) generally showed net immobilization across all temperatures, indicating strong biological nutrient demand.

Additionally, dissolved organic carbon (DOC) experiments suggest that a portion of the observed ecosystem carbon loss is likely related to downward DOC fluxes from the disturbed organic horizon into the underlying mineral layer. Ultimately, these findings indicate that while MSP appears to drive a significant, time-delayed carbon debt through the mineralization of unprotected POM, it does not fundamentally alter the inherent temperature sensitivity (Q_{10}) or proportional SOM fractionation of the surviving carbon pool.

Keywords: Mechanical site preparation (MSP), Soil carbon dynamics, Lichen woodlands, Carbon debt, Soil organic matter fractionation.

2.2 Introduction:

Forests are critical to the global carbon cycle, acting as essential carbon reservoir that help mitigate climate change (Ciais et al., 2013; Friedlingstein et al., 2026; Pan et al., 2011). While forest vegetation acts as an immediate reservoir, forest soils serve as a massive, long-term reservoir, storing approximately 1,700 Gt C globally and nearly four times the amount stored in vegetation (450 Gt C) (Friedlingstein et al., 2026). Among forest types, boreal forests are particularly notable for their thick organic layers, which store substantial amounts of carbon (Mayer et al., 2020). These layers play a key role in carbon sequestration, helping to mitigate climate change by holding significant amounts of carbon estimated at approximately 272 Gt C globally, with average soil carbon stocks ranging from 200 to 300 Mg C ha^{-1} (Bradshaw et al., 2009; Pan et al., 2011). The scientific community has recognized the importance of soil carbon sequestration in mitigating global climate change (Bossio et al., 2020; Lal, 2004). This is particularly the case in boreal regions, where soils are significant carbon reservoirs. Boreal forests store approximately one-third of the world's terrestrial carbon, most of which is in the soil (Pan et al., 2011). As the impacts of climate change intensify, effective forest management practices that support carbon storage are increasingly important (Lal, 2005). In this context, soil health emerges as a central factor in forest productivity and long-term sustainability.

Mechanical site preparation (MSP) is a widely used forestry technique designed to enhance tree growth and forest regeneration, particularly in managed boreal forests (Thiffault et al., 2011). MSP operations invert and mix the soil profile, creating a highly heterogeneous micro-topography characterized by artificially raised organic mounds (M), exposed mineral furrows (F), and adjacent undisturbed inter-furrow (IF)

compartments between machine passes (Marty et al., 2024). Disturbing the boreal forest soils through MSP may affect carbon content, composition, and stability among microtopography structures, thus altering the forest's role as a carbon reservoir (Lafleur et al., 2011; Mäkipää et al., 2023). This makes it essential to investigate how MSP influences soil carbon dynamics, particularly its impact on carbon sequestration processes within boreal ecosystems, as the long-term effects of this practice remain poorly understood especially in boreal forests where organic carbon is primarily stored in soils rather than vegetation (Kurz et al., 2013).

From a global restoration perspective, boreal ecosystems present significant opportunities for climate mitigation, particularly through the afforestation and enhancement of low-density forest landscapes (Boucher et al., 2012; Faubert et al., 2023). In Canada, this biome includes Lichen Woodlands (LWs), which are open ecosystems characterized by sparse tree cover and low soil productivity—conditions that often persist following successive natural disturbances such as wildfires and insect epidemics that hamper natural regeneration (Gonzalez, 2013; Jasinski & Payette, 2005; Payette et al., 2000; Payette & Delwaide, 2018). Because LWs naturally possess inherently low baseline soil organic carbon (SOC) stocks alongside this sparse tree cover, they present a high-potential opportunity for significant relative carbon gains through afforestation, distinguishing them from already carbon-dense, closed-canopy boreal forests. Consequently, LWs are increasingly targeted for afforestation efforts to enhance their capacity as carbon reservoir (Gaboury et al., 2009; Marty et al., 2024). Disturbances like MSP in the LWs are thought to lead to the loss of part of this stored carbon, which may contribute

to global carbon emissions (Botroh et al., 2023). Research has shown that MSP rapidly decreases organic concentration by 105 g kg^{-1} in the disturbed organic layer (Marty et al., 2024). Existing studies have shown inconsistent results regarding the extent to which MSP causes carbon loss or redistribution, leaving a gap in the scientific knowledge of how MSP influences carbon sequestration in LWs (Dufour et al., 2024; Marty et al., 2024; Strömgren et al., 2026). Carbon budget models predict a loss of approximately 3-4 tonnes of carbon per hectare (Gaboury et al., 2009), although these values have rarely been confirmed through field studies (Yu et al., 2023). Recent empirical assessments, however, are beginning to bridge this gap; for instance, Dufour et al. (2024) reported a more conservative carbon debt of 2 t C ha^{-1} following scarification in Quebec LWs. Concurrently, extensive long-term trials in boreal forests have evaluated not only the response of SOC to MSP but also the aboveground carbon component. While initial soil carbon losses often occur following practices like disc trenching, accelerated aboveground biomass growth over the rotation period frequently compensates for these initial belowground deficits (Strömgren et al., 2026). This compensation can promote overall ecosystem carbon stocks without causing substantial long-term reductions in soil carbon, though minimizing disturbance remains necessary to avoid other ecological trade-offs. Quantifying the extent to which MSP affects soil carbon storage, carbon fluxes, and organic matter stability in LWs is essential for understanding the long-term carbon sequestration capacity (Sutinen et al., 2019).

The specific impacts of MSP on SOC composition, soil organic matter (SOM) stability, and nutrient cycling remain uncertain (Marty et al., 2024). Resolving this

uncertainty requires dissecting the soil carbon pool into functional components based on their physical protection and biological availability. Accordingly, SOM is often categorized as particulate organic matter (POM) and mineral-associated organic matter (MAOM) (Benbi et al., 2014). POM consists of partially decomposed plant and animal residues that are relatively large, structurally recognizable, and less chemically protected, making them highly vulnerable to microbial decomposition when physically exposed by soil disturbance (Cotrufo et al., 2019; Lavallee et al., 2020). MAOM on the other hand, is SOM that has bonded with mineral particles, typically clay and silt. This association provides long-term protection against rapid decomposition (Lavallee et al., 2020). While the physical disruption caused by MSP undeniably exposes encapsulated POM to rapid loss, the intensive churning action might simultaneously facilitate the formation of new MAOM by forcing organic matter into direct contact with the underlying mineral layer. The net balance of these opposing pathways remains untested in boreal LWs.

The physical disruption of soil aggregates and the exposure of previously encapsulated SOM fractions induced by MSP have the potential to reduce the ability of these boreal soils to act as carbon reservoir, potentially shifting them toward net carbon sources, at least for a few years. The degree of this impact, however, is still uncertain due to the lack of comprehensive studies that investigate the specific mechanisms and pathways through which MSP affects soil carbon fluxes, and temperature sensitivity of soil respiration (Botroh et al., 2023). Furthermore, the spatial heterogeneity introduced by MSP—such as the creation of mounds and furrows—leads to differing soil microenvironments that complicate our

understanding of carbon distribution and stability in these disturbed areas (Marty et al., 2024). However, the impacts of these structural changes are not static, they represent a temporal trajectory. The initial years following scarification are typically defined by physicochemical destabilization and carbon loss, which may eventually transition into a new phase of stabilization and vegetation re-establishment over time (Marty et al., 2024).

To accurately evaluate the long-term impact of mechanical disturbances, it is crucial to understand the stability of the remaining SOM and its temperature sensitivity, typically expressed as the Q_{10} value. Fundamentally, the Q_{10} coefficient is a broad thermodynamic metric used to quantify the temperature dependence of various chemical reaction rates and biological processes (Mundim et al., 2020). In the specific context of soil ecology, the Q_{10} metric represents the factor by which the microbial respiration rate increases with every 10°C rise in temperature. According to carbon kinetic theory and thermodynamic principles, the temperature sensitivity of SOM decomposition is inversely related to its biochemical reactivity; therefore, more recalcitrant carbon pools generally exhibit higher Q_{10} values because their decomposition requires a higher activation energy (Knorr et al., 2005; Tang et al., 2017). Understanding this dynamic is essential for evaluating how MSP might shift the balance of labile and recalcitrant carbon, thereby altering long-term carbon mineralization under varying temperature conditions.

The primary objective of this study was to assess the impact of MSP on soil carbon dynamics in LWs. To capture the temporal trajectory of these disturbances, we employed a chronosequence approach by sampling two separate sites representing

different time-since-disturbance intervals while one scarified 4 years prior and the other 12 years prior to sampling. This comparative approach allowed us to distinguish between the immediate physicochemical destabilization of soil carbon following mechanical mixing (short-term) and the subsequent phase of potential stabilization and vegetation re-establishment (medium-term) (Sutinen et al., 2019) . Additionally, the aim was to determine whether the reported reductions in carbon concentration in the M sections are mainly due to carbon loss as CO_2 emissions to the atmosphere or if some carbon is transported to the mineral layer through leaching of dissolved organic carbon (DOC) (Marty et al., 2024). The differences in carbon composition and carbon-to-nitrogen (C:N) ratios between disturbed and undisturbed soil sections were examined to assess the degree of microbial processing, evaluate changes in the quality of the remaining organic matter, and estimate the carbon loss. Furthermore, the stability of organic carbon in disturbed and undisturbed soils was evaluated by determining the temperature sensitivity (Q_{10}) of soil respiration. Finally, the fractionation of SOM into POM and MAOM (García-Palacios et al., 2024) was utilized to specifically analyze the stability of organic carbon and quantify the amount of sequestered carbon within the soil.

It was hypothesized that MSP would affect the carbon stock dynamics in the soils of the LWs, including its soil respiration and Q_{10}. It was expected that MSP would lead to a decrease in carbon stock in the soils of the LWs, primarily from the organic horizons of the M compartment. It was also anticipated that the disturbed sections, including both the M and F, would exhibit distinct differences in organic carbon composition and C:N ratios compared to the undisturbed inter-furrow (IF) section,

owing to varying rates of SOM decomposition. Furthermore, it was predicted that soil respiration and Q_{10} would differ significantly between the disturbed and undisturbed sections. While it was anticipated that mechanical disturbances would enhance microbial activity and organic matter decomposition—leading to increased CO_2 emissions—the resulting Q_{10} values would vary depending on the recalcitrance of the remaining carbon, consistent with the thermodynamic principles. Additionally, MSP was expected to facilitate carbon fluxes from the disturbed soil sections to the underlying mineral layer, resulting in alterations to overall carbon storage and cycling. Finally, regarding the time-dependent evolution of these dynamics, it was predicted that carbon losses driven by enhanced microbial respiration and DOC leaching would be significantly more pronounced in the older scarified site (12 years) compared to the recent site (4 years), with the older site expected to show signs of physicochemical stabilization and reduced mineralization rates as it reaches a new equilibrium.

2.3 Material and methods

2.3.1 Site Description and experimental design

The study was conducted in two LWs located in the Saguenay–Lac-Saint-Jean region of Québec, Canada. The first site underwent MSP in 2012 (50.28° N, 72.37° W), while the second was scarified in 2020 (48.46° N, 73.06° W). Both sites are characterized by their coarse-textured soils and sparse tree cover, typical of open LWs. The exact locations of the sites are shown on Figure 2 (Marty et al., 2024). The region experiences a sub-arctic or continental climate characterized by cold winters (average January and February temperatures of −20° C) and warm summers

(average July temperatures of +16° C). The mean annual temperature is approximately 0° C, with a mean annual precipitation of 960 mm, of which about 33% falls as snow (Marty et al., 2024).

The soils at both sites are well-drained humo-ferric Orthic or humo-ferric Ortstein Podzols, developed from glacial or fluvio-glacial till derived from Precambrian charnockitic gneiss. These soils are characteristically coarse to fine sands featuring a relatively thin organic layer (typically < 15 cm) and low base cation concentrations (Marty et al., 2024; Ouimet et al., 2018). The local vegetation is typical of LWs resulting from successive wildfires, predominantly featuring ericaceous shrubs such as *Rhododendron groenlandicum*, *Kalmia angustifolia*, and *Vaccinium angustifolium*, interspersed with ground dwelling lichens of the *Cladonia* genus. Neither of these specific experimental sites was afforested following the MSP, ensuring that any observed changes in soil properties can be attributed solely to the physical disturbance of the MSP (Marty et al., 2024).

The experimental design consisted of three distinct blocks established at each site, separated by a distance of at least 300 m. Within each block, three sampling plots were delineated. The M consisted of displaced soil, moved during MSP, and original soil, which remained in place beneath. The F was the area from which soil was removed, and the IF was the undisturbed section.

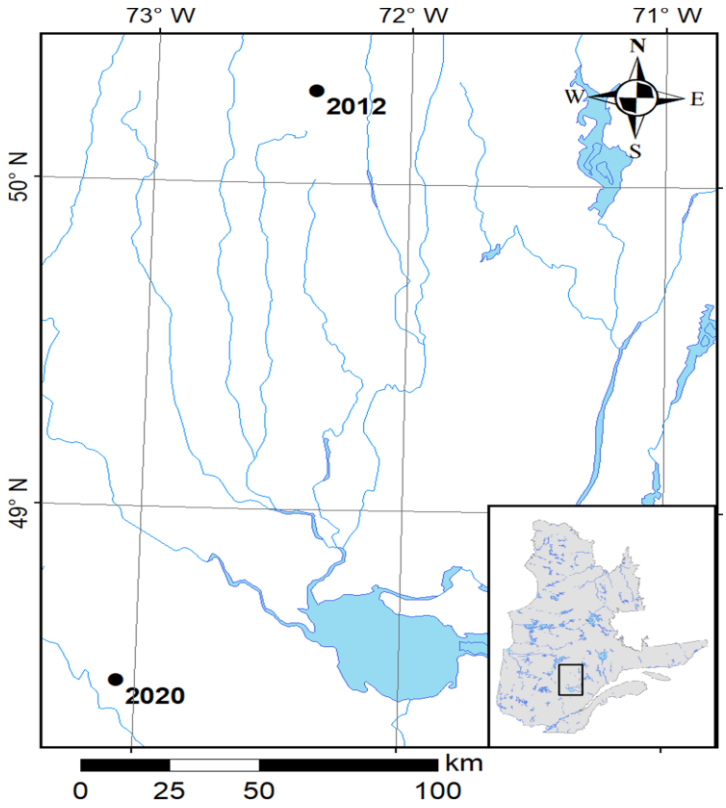

Figure 2: Location of the two studied boreal lichen woodlands in the Saguenay–Lac Saint-Jean region of Québec, Canada: the one scarified in 2012 (2012 site) and the one scarified in 2020 (2020 site) (Marty et al., 2024).

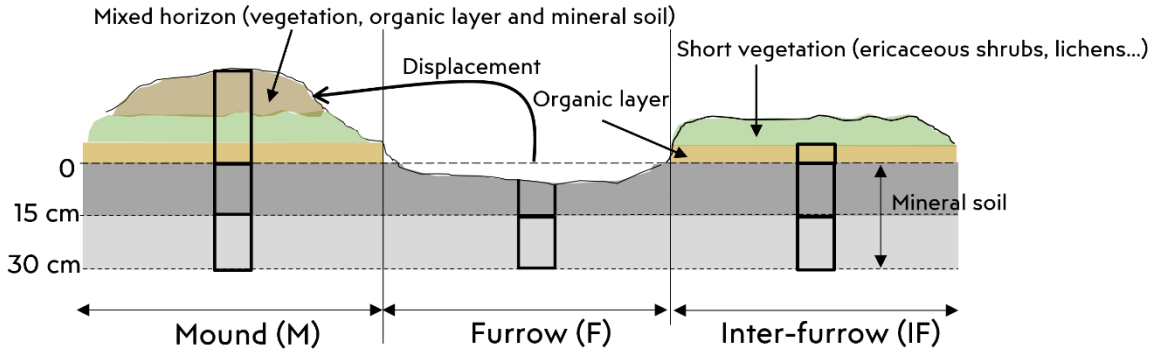

Figure 3: Schematic representation of the three compartments created by mechanical site preparation (Marty et al., 2024).

2.3.2 Sample collection

Soil sampling was conducted during the summer of 2024. The experimental design yielded a total of 54 organic layer soil samples and 18 mineral layer soil samples across the two sites. Organic layer soil samples were collected from the mounds (M) and inter-furrows (IF) across all three plots within every block (2 sites × 3 blocks × 3 plots). A 30 × 30 cm frame (Figure 4) was used to delineate the area; the organic horizon was cut using a handsaw, carefully removed with a shovel, and bagged for transport. This sampling yielded 18 IF organic samples and 18 M organic samples. During subsequent laboratory processing, the 18 M organic samples were further separated into their two distinct constituent organic layers. The inverted displaced organic material on top and the buried original organic material beneath resulting in 36 M organic samples, for a total of 54 organic samples (36 M and 18 IF organic samples).

For the mineral layer, soil samples from the top 0–15 cm were collected using a stainless-steel soil corer (15 cm depth, 8 cm diameter). Mineral layer soil was collected from only one randomly selected plot per block. Within each of these selected plots, one core was taken from each of the three compartments (M, F, and IF), resulting in 18 total mineral layer soil samples (6 M, 6 F, and 6 IF).

Finally, to facilitate the analysis of dissolved organic carbon (DOC) leaching, intact soil cores were collected to preserve the natural soil structure. From both the 2012 and 2020 sites, one M and one IF soil core were sampled from one representative plot per block (yielding 6 DOC cores per site, for a total of 12 cores). These were

extracted using an AMS Soil Core Sampler (AMS Inc., American Falls, ID, USA) equipped with a 5 cm (2-inch) diameter plastic liner.

Figure 4: Photographs of soil core sampling (left panel) and bulk soil sampling (right panel) (Photos by Carbone boréal, 2024).

2.3.3 Pretreatment of soil samples

The collected soil samples underwent a series of pretreatment steps to prepare them for laboratory analyses (Figure 5). The organic layer soil samples collected from the M compartment were separated into two parts: “displaced” soil, which is the soil turned over during the process of scarification, and the underlying “original” soil, which was already present in the M compartment before the process of scarification. The organic layer soil samples from IF compartment served as the control, representing the undisturbed section. The above-ground biomass and the below-ground biomass were removed from all the collected organic layer soil samples and put aside. Since the mineral layer is beneath the organic layer, there was no above-ground biomass, but some below-ground biomass was removed and weighed. Then, all the soil samples were sieved, the organic layer soil samples were first sieved using a 5-mm sieve to remove larger biomass and then using a 2-mm sieve to remove smaller biomass. The mineral layer soil samples were sieved once using a

2-mm sieve to remove coarse sand. The biomass fractions were oven-dried at 55°C for 48 hours and the < 2 mm soil fractions were air-dried in a drying room for 5 days then weighed using a scale.

Figure 5: The separation (left panel), 5-mm sieving (middle panel), and 2-mm sieving (right panel) of the soil samples.

2.3.4 Grinding of soil samples

About 20 g of air-dried organic and mineral layer soil samples were ground for laboratory analyses. First, the soil samples were placed in 50-mL centrifugal tubes (Figure 6), and each tube was filled with three metal balls. The centrifugal tubes were then closed tightly. The tubes were packed in a tumbler and soil was ground for 72 hours. This grinding process resulted in fine powder samples, which were used for carrying out laboratory analyses (Marty et al., 2024; San-Emeterio et al., 2023).

Figure 6: Homogenized grinded soil samples prepared for elemental analysis (Photo by David Simard, 2025).

2.3.5 Field capacity of soil

The field capacity of soil is a measure of the soil's ability to retain water after it has been saturated and excess water has drained away, which is crucial for assessing soil moisture availability for plants and soil microorganisms (Brady, 2016; Cassel & Nielsen, 1986). First, the air-dried and homogenized soil samples were placed in 50-mL centrifugal tubes with a hole drilled at the bottom to allow water to drip out (Figure 7). Then the soils were saturated with water and then the tubes were left to drip any excess water for 4 hours. The wet soil was weighed using a precision scale, then dried in an oven at 105°C for 20 hours before being weighed again. Field capacity was calculated as follows:

$$Field\ Capacity\ (ml\ per\ g\ of\ soil) = \frac{Wet\ Soil\ (g) - Oven\ dried\ Soil(g)}{Oven\ dried\ Soil\ (g)} \qquad [1]$$

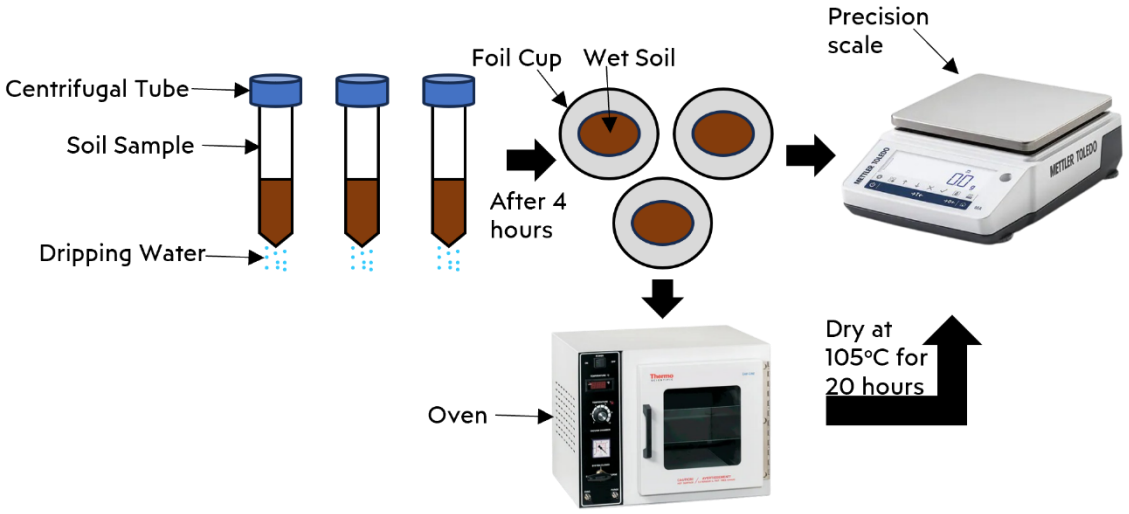

Figure 7: Laboratory procedure for determining soil field capacity.

2.3.6 Residual water of soil

Residual water in soil samples was measured immediately before analysis or before sealing the sample in a hermetic container to account for any remaining moisture that could lead to an underestimation of actual carbon concentration.

First, 5-10 g of soil stored at room temperature was weighed using a scale, and then the soil was dried in an oven at 105°C for 20 hours before being weighed again. The formula used to calculate the residual water was:

$$Residual\ Water\ (ml\ per\ g\ of\ soil) = \frac{Undried\ Soil\ (g) - Oven\ Dried\ Soil(g)}{Oven\ Dried\ Soil\ (g)} \quad [2]$$

And to obtain the actual dry mass of the soil, the formula used was:

$$Dy\ mass\ of\ soil\ (g) = Undried\ Soil\ (g) * (1 - Residual\ water)\ (ml) \quad [3]$$

2.3.7 Laboratory analyses

The chemical analyses included carbon and nitrogen content, C/N ratios, SOM fractionation, soil respiration rates, and dissolved organic carbon.

2.3.7.1 Total Organic Carbon and Nitrogen

The total carbon and total nitrogen contents of all the organic and mineral layer soil samples were measured using an organic elemental analyser which was calibrated using BBOT (CHNS; Flashsmart CHNS by thermos fischer scientific) (PerkinElmer, 2010). First, a small amount of dry ground soil sample (around 5 mg for organic layer soil and 50 mg for mineral layer soil) was weighed in a tin capsule using a high precision scale. The soils in the capsules were then treated with 20 µL of H_2SO_3 (6 %) at 70°C heated for 20 hours to remove the inorganic carbon (Kennedy et al., 2005; Verardo et al., 1990). Then, the tin capsule was packed and introduced into a combustion chamber where it was combusted at high temperatures (around 950-1000°C) in the presence of an oxidizer gas (oxygen). This oxidizes the sample, converting organic carbon into CO_2, and organic nitrogen into NOx and then reduced to N_2. These gases are then carried through a chromatography column by a carrier gas (helium). The CHNS (Figure 8) uses the detected chromatogram peaks to quantify the carbon and nitrogen contents in each sample, applying standard parameters optimized for soil carbon analysis (Dhaliwal et al., 2011; PerkinElmer, 2010).

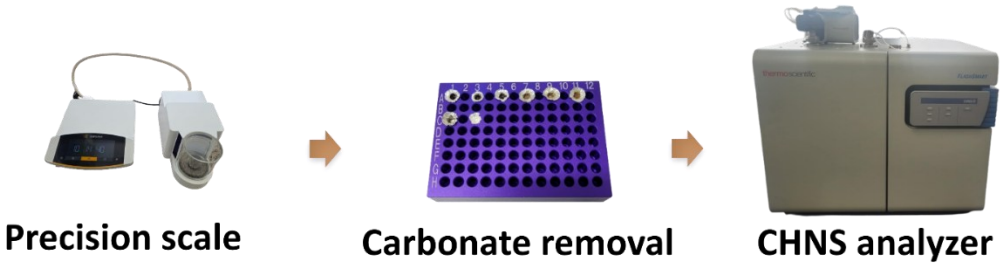

Figure 8: Laboratory procedure of analysing organic Carbon and Nitrogen.

Using the total carbon and nitrogen values, the C/N ratio were calculated, which is an indicator of the level of decomposition of soil organic matter (SOM) (Klopp, 2024).

2.3.7.2 Soil organic matter fractionation

The SOM fractionation was carried out for all the organic and mineral layer soil horizons by a combination of density and filtration fractionation. Although physical fractionation into POM and MAOM is conventionally reserved for mineral layers, it was deliberately applied to the organic horizons in this study. Because MSP physically incorporates underlying mineral particles into the displaced organic layer, effectively blurring traditional horizon boundaries, this fractionation was essential to accurately isolate and quantify any newly introduced mineral associated carbon from the unprotected particulate pools.

The soil samples (< 2 mm) were treated in a dense solution (1.6 g cm^{-3}) of sodium iodide (NaI) to apply a fractionation of the SOM based on density (Benbi et al., 2012). Since POM has a lower density than the solution (density < 1.6 g cm^{-3} and particle size > 53 µm) (Lavallee et al., 2020; Paré & Bedard-Haughn, 2011), it floats to the top, forming the supernatant. This floating POM was aspirated using the Nalgene filtration setup, rinsed two to three times with 50 mL aliquots of distilled water to remove the NaI solution, dried at 60°C, and weighed for mass determination.

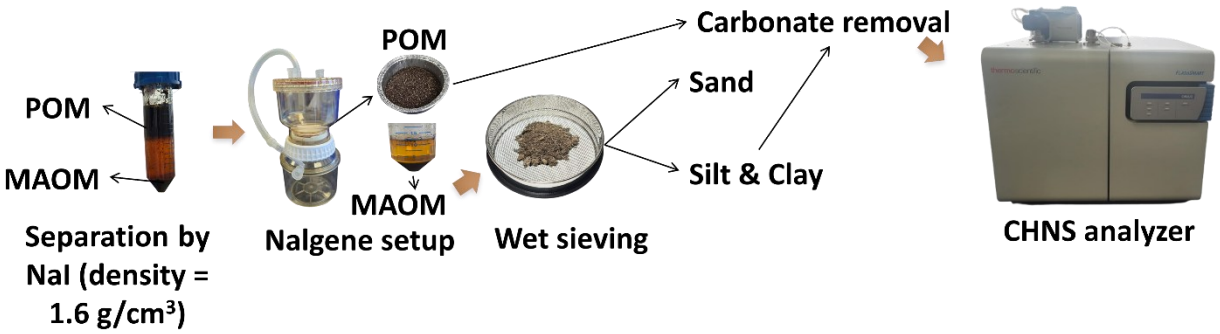

Figure 9: Workflow for density and physical fractionation of soil organic matter into Particulate organic matter (POM) and Mineral associated organic matter (MAOM) using NaI (1.6 g cm^{-3}), followed by wet sieving and CHNS analysis for carbon and nitrogen quantification.

MAOM has a higher density (particles > 1.6 g cm^{-3} and size < 53 µm) and will thus remain at the bottom of the centrifuge tube. It was retrieved by wet sieving the remaining heavy fraction soil with distilled water using a 53 µm sieve that separates the heavy fraction into sand (> 53 µm) and silt-clay fraction (< 53µm). The MAOM fraction was dried and weighed similarly to the POM fraction (Poeplau et al., 2018). Then the dried POM and MAOM fractions were then ground into fine powder and treated for carbonates and analysed for their organic carbon and nitrogen contents (Figure 9).

2.3.7.3 Soil respiration, decomposition and mineralization rates

The assessment of soil respiration rate will clarify MSP effects on microbial activity and organic matter decomposition in disturbed and undisturbed sections of LWs. This was done by measuring the rate of CO_2 emissions from the soil (an indicator of microbial respiration) and nitrogen mineralization under controlled conditions (Marty et al., 2024). Both organic and mineral layer soil samples collected from different

sections (M, F and IF) of both the 2012 and 2020 sites were analyzed for soil respiration rates.

- Incubation setup (Figure 10):

The incubation was conducted using 500 ml sealed Mason jars as incubation chambers. The jars were placed in incubation chambers at three controlled temperatures (15°C, 22°C, and 30°C) in sequential 21-day runs. These specific temperature steps were utilized to establish the full thermal range necessary for calculating the temperature sensitivity (Q_{10}) of soil respiration. For a given temperature run, a total of 117 jars were incubated simultaneously. This consisted of the 36 unique soil samples (18 organic and 18 mineral) each replicated three times (108 jars), alongside 9 blank jars (i.e., empty jars) to account for background CO_2. Inside each of these 117 Mason jars, the soil was distributed across four separate vials, with each vial holding either 2.5 g (for the organic horizon) or 4.5 g (for the mineral horizon) of the < 2 mm dry soil fraction. Prior to sealing, soil moisture in the vials was adjusted to 40% of field capacity, and 10 ml of water was added to the bottom of each Mason jar to maintain constant air humidity levels. The 40% moisture threshold was selected to closely mimic the naturally well-drained, ambient moisture regimes characteristic of the coarse-textured, sandy soils typical of boreal lichen woodlands, while simultaneously preventing the artificial anaerobic conditions that often occur at standard, higher water saturations within highly porous organic matrices. This four-vial system allowed us to sequentially remove and analyze one vial at each designated time interval (3, 4, 5, and 9 days). The 21-day total incubation period was specifically chosen because it provides a sufficient temporal window to

capture the peak active mineralization kinetics of the highly vulnerable labile carbon pools freshly exposed by the physical disturbance, without the microbial communities entering an extended, substrate-limited starvation phase. Once a 21-day incubation run was completed for one temperature, a fresh set of 117 jars was prepared using new aliquots from the same 36 soil samples, and the entire process was repeated for the next temperature setting.

Figure 10: Sealed incubation chamber for measuring soil microbial respiration.

- Measurement of CO_2 emissions:

To quantify the accumulated CO_2 in the headspace, we utilized an EGM-5 Portable CO_2 Infra-Red Gas Analyzer (PP Systems, Amesbury, MA, USA) (Figure 11). This device is widely recognized in soil science for its accuracy in measuring gas concentrations via infra-red gas analysis (PPSystems, 2023). For this experiment, the analyzer was factory-calibrated specifically for a measurement span of 0 to 10,000 ppm. Within this selected range, the device maintains a stated accuracy of 1% of the total span, corresponding to a uniform uncertainty of ±100 ppm across all measured concentrations. The sampling procedure followed a manual injection

protocol to ensure a representative measurement of the jar's headspace. First, to account for gas stratification within the jar, the headspace air was thoroughly mixed using a 20 ml syringe by drawing and expelling the air five times. Subsequently, a 10 ml aliquot of the mixed gas was extracted and injected into the EGM-5 through a specialized injection port. Upon injection, the analyzer circulates the gas sample through its optical bench, where CO_2 molecules absorb infrared light at a specific wavelength (4.26 µm). The device continuously monitors the absorbance and converts it into a concentration value using an internal linearization algorithm. This process includes automatic corrections for ambient temperature and atmospheric pressure to ensure accuracy. The measurement cycle for each injection typically lasts until a stable peak concentration is reached, which generally occurs within a few seconds of injection. The final CO_2 concentration (in ppm) was recorded once the reading stabilized. The mean values obtained from three blank jars (incubated without soil) were subtracted from the sample readings for each batch.

EGM-5 Injection setup

Figure 11: Gas sampling and analysis setup using an EGM-5 CO_2 analyzer.

- Nitrogen and Phosphorus mineralization:

To determine the mineralization rates of nitrogen and phosphorus, sampling was performed at each designated time interval by removing one of the four vials from each incubation jar. The soil from the removed vial was transferred to a 50 ml Falcon tube for chemical extraction. A 0.1 M $CaCl_2$ solution was added to each tube to achieve a 1:10 soil-to-solution ratio, requiring 25 ml of solution for organic layer soil samples (2.5 g) and 45 ml for mineral layer soil samples (4.5 g). To ensure complete interaction between the soil and the extractant, the tubes were secured flat on a mechanical shaker and agitated at 160 rpm for 30 minutes. Following agitation, the suspension was filtered through Cytiva Whatman Grade 2 qualitative filter paper (8 µm pore size) into 15 ml collection tubes to remove particulates (Figure 12). The resulting clear extracts were then analyzed for inorganic nitrogen, specifically ammonium (NH_4^+) and nitrate (NO_3^-) and available phosphorus (PO_4^{3-}) concentrations using a Gallery Plus (Thermo Fisher Scientific) (Butnan & Vityakon, 2020). To calculate the net mineralization and immobilization rates, the change in these extractable nutrient concentrations was determined over time. For each interval, the concentration of inorganic nitrogen (total $NH_4^+ + NO_3^-$) or available phosphorus measured at the previous time point was subtracted from the concentration measured at the current time point. A positive difference indicated net mineralization (the microbial release of inorganic nutrients into the soil), while a negative difference indicated net immobilization (the microbial uptake and assimilation of those nutrients). These concentration changes were then divided by

the duration of the respective time interval to express the final net rates as µg of nutrient per g of dry soil per hour (µg g^{-1} h^{-1}).

Figure 12: Filtration setup for soil extract analysis.

- Gallery Plus analysis:

The clear extracts were analyzed using a Thermo Scientific Gallery Plus (Figure 13), an automated photometric sequential analyzer. This system allows for high-throughput, precise quantification of nutrient concentrations. From each filtered extract, a 2 mL aliquot was transferred to analysis buckets. The Gallery Plus software was programmed to perform three primary tests. Ammonium (NH_4^+) to determine the initial stages of nitrogen mineralization. Total Oxidized Nitrogen (TON) to measure the concentration of nitrates and nitrites, indicating the extent of nitrification within the disturbed soil. Phosphorus (PO_4^{3-}) to quantify the soluble phosphate released during the incubation (Williamson et al., 2024). The formal method detection limits (MDL) for these assays were 0.0005 mg L^{-1} for ammonium, 0.00035 mg L^{-1} for TON, and 0.00036 mg L^{-1} for phosphorus and were calibrated using TON, ammonium and phosphorus standards.

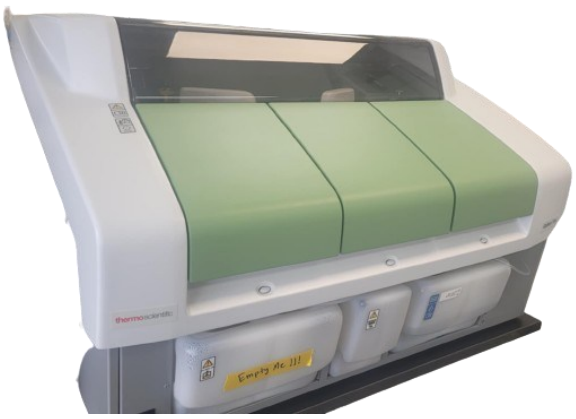

Figure 13: Thermo Scientific Gallery Plus.

2.3.7.4 Dissolved organic carbon analysis

Dissolved organic carbon (DOC) leaching was assessed using intact soil cores collected from disturbed (M) and undisturbed (IF) compartments at both study sites. This approach was used to determine how MSP influences the leaching of DOC in LWs. Soil profiles were selected because they maintain the natural structural integrity, hydraulic routing, and localized DOC dynamics that are inherently lost during soil homogenization (Kalbitz et al., 2000; Qualls & Haines, 1992).

To replicate the complex structure of the M compartment in the laboratory, soil columns were constructed by stacking separate soil cores representing the three distinct layers, namely the displaced soil (soil overturned by the scarifier), the buried original organic surface, and the underlying mineral layer (0–15 cm). Similarly, the IF profiles were assembled by stacking two intact cores corresponding to the natural organic horizon.

- Experimental setup:

The individual soil column sections were connected in series using 1/4-inch (0.635 cm OD, 0.43 cm ID) tubing and T-connectors. Crucially, hose clamps were installed on the T-connector side ports to serve as sampling valves, enabling the collection of leachate samples between each soil core. This configuration allowed DOC to be measured after each soil horizon, enabling us to track how soluble carbon changed as water passed from the organic layer through displaced material and into mineral layer (Chantigny, 2003; Moore et al., 2008). Deionized water (DI) was used as the percolating solution. A Mariotte bottle system provided constant hydraulic head, ensuring stable and gravity-driven flow through the soil columns (Ogden et al., 2017) (Figure 14). Flow rates were measured periodically by recording water volume exiting each column over time.

Figure 14: Experimental setup for leaching dissolved organic carbon (DOC).

Leaching was initiated by applying approximately 1.5 to 2 L DI water to the top of the first column in each assembly. Water percolated vertically through successive soil horizons, and leachate was collected separately at the outlet of each column. This design simulates vertical porewater movement under flow conditions typical of boreal forest soils, while enabling horizon-specific DOC characterization (Kalbitz et al., 2000). Leachate from each outlet was collected in acid washed glass containers immediately after appearance. To isolate dissolved carbon, all samples were filtered through 0.45 µm syringe filters, a standard threshold that removes particulate organic matter while retaining DOC (Jones & Willett, 2006) (Figure 15). Filtered leachates were stored at 4°C before being shipped to an accredited external laboratory (Groupe de Recherche Interuniversitaire en Limnologie- Université du Québec à Montréal) for DOC quantification. Samples were analyzed using an OI Analytical Aurora 1030W TOC Analyzer following a wet heated persulfate oxidation method. Inorganic carbon was first removed by adding 5% phosphoric acid at 70°C. The remaining organic carbon was then oxidized by adding 10% sodium persulfate and heating the sample to 98°C. The resulting CO_2 evolved from this reaction was subsequently quantified using a nondispersive infrared (NDIR) sensor. This analytical method maintains a measurement precision of ≤ 5% and an operational range of 0.1 to 100.0 mg L^{-1} (DelSontro et al., 2016).

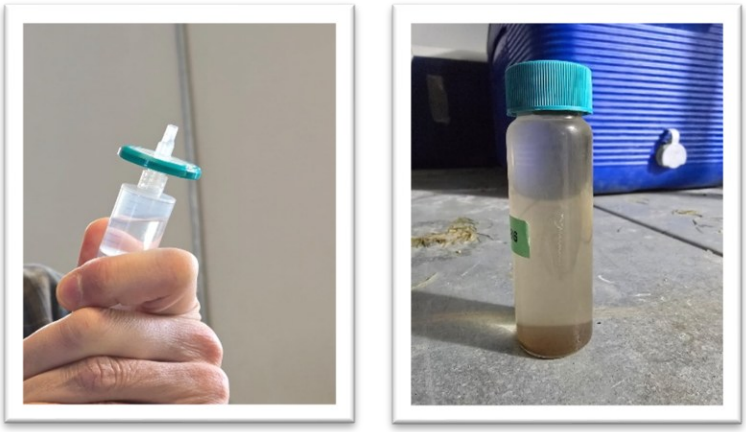

Figure 15: Final filtration (left panel) and storage of dissolved organic carbon (DOC) samples (right panel).

2.3.8 Drone imagery and spatial analysis

Drone imagery was utilized to accurately assess the spatial distribution of the microtopography and soil displacement across the study plots. A DJI M300 RTK drone captured high-resolution images of each block and plot within the study sites (Figure 16) (Yang et al., 2021). The primary objective of this process was to determine the exact surface covered by the M, F, and IF sections created by the MSP. These images were processed using Fiji (previously known as ImageJ) (Schindelin et al., 2012). This spatial information is critical for applying an upscaling factor to each parcel within all the blocks, accounting for soil that was turned over during the MSP process (Marty et al., 2024). Specifically, we selected individual drone images corresponding to a ground surface area of approximately 100 m^2 for each plot. By incorporating this correction factor, we aimed to improve the accuracy of the study's results regarding soil carbon dynamics and distribution (Liu et al., 2022). Additionally, knowing the relative surface area of each compartment is crucial for estimating carbon loss on a larger scale within the LWs (Marty et al., 2024).

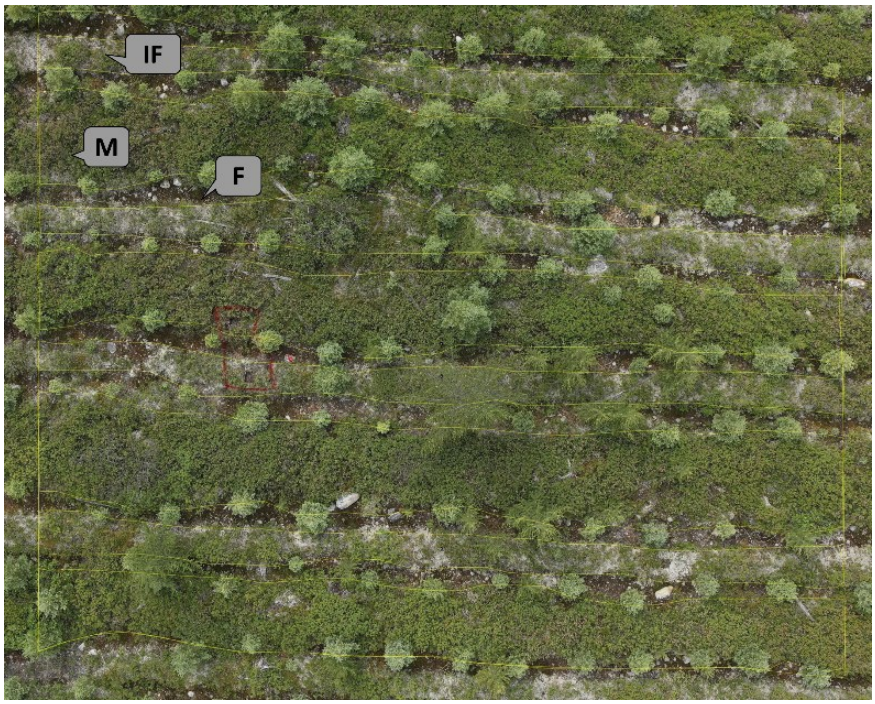

Figure 16: Sample of Image processing in Fiji for surface cover estimation of compartment Inter-Furrow (IF), Mound (M) and Furrow (F).

Each image was processed to quantify the relative surface area of the compartments (Figure 16). For each scarification pass, two F, one IF, and two half M are produced, resulting in approximately twice as many F polygons as M or IF polygons in the region of interest (ROIs). We maintained this ratio during our image analysis to ensure a proportional representation of the site. Using the polygon selection tool in Fiji, the boundaries of individual soil compartments were manually traced. The Fs were delineated first, followed by the IFs and Ms. Once defined, the ROIs were measured to calculate the area of each compartment in pixel units. These values were then exported to calculate the relative percentage cover of each compartment (M, F, IF) within the plot, providing the necessary weighing factors for our stand-scale carbon calculations (Marty et al., 2024).

This workflow provided a reproducible and accurate method to quantify the proportional surface area of M, F, and IF compartments within each plot. These factors were later applied to estimates the carbon stock to account for spatial heterogeneity introduced by MSP.

2.3.9 Statistical analyses and calculations

2.3.9.1 Carbon loss calculation

The total carbon stock of each soil compartment (M, F, and IF) (C_{stock}; kg C m^{-2}) was calculated using the following equation:

$$C_{stock} = \frac{(CF \times BM_{total}) + (M_{soil} \times C_{soil})}{A} \qquad [4]$$

where CF is the carbon fraction of dry biomass (0.5). BM_{total} is the total dry biomass, calculated as the sum of aboveground and belowground biomass (kg). M_{soil} and C_{soil} are the total dry weight and the total carbon concentration of the < 2 mm fraction of the organic horizon (kg), respectively. A is the surface area of the sampling frame (m^2).

2.3.9.2 Calculation of Carbon Loss at the Stand Scale

To estimate the net carbon loss at the stand scale (landscape level), we calculated the carbon stock across the three compartments (M, F, IF) and subtracted the baseline carbon stock of the undisturbed IF compartment. Both methods utilized the proportional area coverage (p) of each compartment determined via drone imagery, where $p_F + p_M + p_{IF} = 1$. The general equation for stand-scale carbon change (ΔC) was:

$$\Delta C = (p_F \times C_F + p_M \times C_M + p_{IF} \times C_{IF}) - C_{IF} \qquad [5]$$

The complexity in this calculation arises from the M compartment, which consists of two distinct layers: the displaced layer on top (M_d) and the buried original layer beneath it (M_{or}). Because the displaced soil can spread outwards post scarification, the surface area of the M can be larger than the surface area of the F from which the soil was extracted ($p_M > p_F$). To account for this spatial discrepancy, we applied two distinct calculation methods based on different structural assumptions regarding the buried M_{or} layer.

- Method 1:

This method assumes that the entire spatial footprint beneath the displaced M (p_M) behaves uniformly as the disturbed M_{or} compartment. The total carbon stock of the M is calculated as the sum of the displaced layer and the original layer across the entire M area. The net carbon change was calculated as:

$$\Delta C_{Method1} = (p_F \times C_F + p_M \times C_{Md} + p_M \times C_{Mor} + p_{IF} \times C_{IF}) - C_{IF} \qquad [6]$$

Because M_{or} generally exhibited a lower carbon stock than the undisturbed IF due to compaction and disturbance, applying the larger p_M area factor to M_{or} likely overestimates the total landscape carbon loss.

- Method 2:

This method accounted for the lateral spreading of the displaced soil. It assumed that only a central area equal to the F's origin (p_F) altered the underlying organic layer soil into M_{or}. The remaining "edges" of the wider M (p_M - p_F) were assumed to

simply rest upon essentially undisturbed IF soil. By replacing a portion of the degraded M_{or} footprint with the baseline C_{IF} value, the net carbon change was calculated as:

$$\Delta C_{Method2} = (p_F \times C_F + p_M \times C_{Md} + p_F \times C_{Mor} + (p_M - p_F) \times C_{IF} + p_{IF} \times C_{IF}) - C_{IF} \quad [7]$$

For both methods, negative values indicate a net loss of carbon from the ecosystem, while positive values indicate a net gain.

2.3.9.2 Data transformation for CO_2 accumulation

The transformation of raw volumetric data into mass-based cumulative carbon mineralization was conducted through a series of mathematical adjustments designed to account for environmental variables and physical gas properties. Initially, the CO_2 concentration attributable solely to microbial respiration was isolated by subtracting the mean concentration of the control blanks C_{blank} from the concentration measured in each sample jar C_{sample}, yielding the net concentration change.

$$\Delta C = C_{sample} - C_{blank} \quad [8]$$

This volumetric ratio, expressed in parts per million (ppm), was subsequently converted into a physical mass of carbon (M_C) using the Ideal Gas Law. This step was critical to account for the fact that the density and molar volume of gas change significantly with temperature. To standardize these measurements across the three incubation temperatures, temperature-dependent correction factors (k_T) were applied to the 500 ml headspace volume of the jars and was calculated using the following equation:

$$k_T = \frac{(\frac{M_{CO2}}{M_{air}})}{(\frac{P \times M_{CO2}}{R \times T})} \qquad [9]$$

Where M_{CO2} is the molar mass of carbon dioxide (44.01 g mol^{-1}), M_{air} is the molar mass of air (28.97 g mol^{-1}), P is the atmospheric pressure, R is the ideal gas constant, and T is the incubation temperature in Kelvin. Using the equation, these k_T factors were applied 0.81 for 15°C, 0.83 for 22°C, and 0.86 for 30°C, corrected for the thermal expansion of the gas, allowing the mass of carbon (m_C; µg) to be calculated as follows:

$$m_C = \frac{\Delta C}{k_T} \times V_{hs} \qquad [10]$$

Were the V_{hs} is the headspace volume of the mason jars. Once the mass of mineralized carbon was quantified in micrograms (µg C), it was normalized to derive the instantaneous respiration rate (R_C; µg C-CO_2 g^{-1} C h^{-1}) and it was calculated as follows:

$$R_C = \frac{m_C}{t \times m_{soil}} \qquad [11]$$

Were the normalization accounted for both the duration of the specific incubation interval (t) and the specific mass of total organic carbon contained within the soil tubes residing inside the Mason jar (m_{soil}), ensuring that the activity levels were comparable regardless of the sample weight or carbon concentration.

Finally, to characterize the total carbon loss over the entire experimental period, these periodic respiration rates were integrated to determine the cumulative carbon mineralized C_{cumul}. This was achieved by summing the carbon produced during

each individual measurement interval (i) up to the final measurement point (n). By multiplying the rate calculated for each interval by the specific time elapsed between samplings Δt_i the total progress of carbon mineralization was tracked over time, and it was calculated as follows:

$$C_{cumul} = \sum_{i=1}^{n}(R_{C,i} \times \Delta t_i) \qquad [12]$$

This cumulative approach allowed for a comprehensive assessment of the total respiration of the SOM under different temperature and compartments.

2.3.9.3 Temperature Sensitivity (Q_{10}) Modeling

The Q_{10} value is a metric used to estimate how much the rate of soil respiration increases with every 10°C rise in temperature. It is calculated using the Van't Hoff equation:

$$\mathrm{R(T)} = \mathrm{R(T_{ref})} \times \mathrm{Q_{10}}^{\frac{\mathrm{T-T_{ref}}}{10}} \qquad [13]$$

Where R(T) describes the temperature sensitivity of respiration, T is the temperature (°C), $\mathrm{T_{ref}}$ is the reference temperature (°C) (Manzoni et al., 2012; C. Marty et al., 2019).

In this experiment, the Q_{10} was derived from a first-order exponential model, which relates respiration rate to incubation temperature following well-established kinetic theory for microbial decomposition (Davidson & Janssens, 2006; Lloyd & Taylor, 1994).

The respiration rate RR was modeled as:

$$RR = b \times e^{\boldsymbol{k}T} \quad [14]$$

Where RR is measured soil respiration rate ($C_{cumul};$), b is basal respiration at temperature T = 0°C, k is temperature coefficient describing the sensitivity of respiration to temperature and T is incubation temperature (15°C, 22°C, or 30°C). The model parameters b and k were estimated for each sample through a non-linear least squares method using the nls () function within the stats package of the R computing environment (R Core Team, 2023).

Once the specific empirical k value was extracted from the incubation data for a given sample, the Q_{10} value, representing the multiplicative increase in respiration for a 10°C rise in temperature, was derived as:

$$Q_{10} = e^{10\boldsymbol{k}} \quad [15]$$

Because the k variable is intrinsically linked to the physical incubation measurements, calculating Q_{10} separately for each soil compartment and site allowed for a direct, data driven comparison of microbial temperature sensitivity between the disturbed and undisturbed soils.

2.3.9.4 Calculation of Nitrogen and Phosphorus Mineralization

To quantify the net mineralization and cumulative release of nitrogen and phosphorus over the incubation period, specific rates were calculated based on the extractable nutrient concentrations. The specific nitrogen mineralization rate ($Rate_N$) for each time interval was calculated by standardizing the extracted concentration against the initial nitrogen content of the soil and was calculated as:

$$Rate_N = \frac{[c] \times V_{ext}}{Mass_{soil} \times \left(\frac{\%N}{100}\right) \times t} \quad [16]$$

Similarly, the specific phosphorus mineralization rate ($Rate_P$) for each interval was calculated as:

$$Rate_P = \frac{[c] \times V_{ext}}{Mass_{soil} \times \left(\frac{\%P}{100}\right) \times t} \quad [17]$$

Where, [c] is the nutrient concentration measured in the extractant. V_{ext} is the volume of the extractant solution used, $Mass_{soil}$ is the dry mass of the incubated soil sample, %N is the total initial nitrogen percentage of the soil sample and %P is the total initial phosphorus percentage of the soil sample and t is the duration of the specific incubation interval.

To establish an accurate baseline and account for the initial, rapid flush of readily available nutrients often observed at the onset of physical soil incubations, the mineralization rates measured at the first interval (Day 3) were treated as the base value. This three-day threshold was selected to isolate and exclude the artificial burst of microbial respiration and mineralization caused by the physical disturbance and rewetting of the soils during laboratory preparation, a well documented phenomenon known as the Birch effect (Birch, 1958; Fierer & Schimel, 2002). To calculate the adjusted cumulative mineralization over the entire 21-day incubation period, this Day 3 baseline ($Rate_{Day3}$) was subtracted from all subsequent interval measurements before summing them and was calculated as follows:

$$Cummulative\ Rate = \sum(Rate_i - Rate_{Day3}) \quad [18]$$

Where $Rate_i$ represents the mineralization rate measured at each respective subsequent interval (i).

2.3.9.5 Statistical analyses

Statistical analyses were performed to evaluate the effects of MSP on soil carbon dynamics, soil respiration, and dissolved organic carbon across the two study sites. Linear mixed-effects models (LMMs) were used as the primary analytical framework, as they allow for the simultaneous assessment of fixed treatment effects while accounting for the hierarchical and spatial structure of the experimental design (Gelman & Hill, 2006; Militino, 2010).

LMMs were fitted to test the effects of compartment (M, IF, F), site (2012 vs. 2020), and their interaction on soil carbon variables (total C, C/N ratios, SOM fractions, and DOC concentrations). The fixed-effects structure of each model included compartment (three levels: M, IF, F), site (two levels: 2012 and 2020), and Compartment × Site interaction, to determine whether the effect of MSP on soil properties differed between sites. The experimental design consisted of 3 replicate blocks per site, with 3 plots nested within each block (n = 9 plots per site), yielding a total of 18 independent plots across the entire study. As plots were nested within blocks, and block-level environmental heterogeneity could influence soil properties, Block was included as a random effect. This accounts for non-independence among samples originating from the same spatial block and improves model generalization across the landscape (Burghoff, 2016).

Model diagnostics (normality of residuals, homoscedasticity, and influence points) were evaluated prior to interpretation by using the DHArma package (Hartig, 2024). When necessary, variables were log-transformed to meet model assumptions.

All statistical analyses were performed using R (R Core Team, 2021) using packages lme4, nlme, and emmeans. Model significance was assessed at $\alpha=0.05$, and post-hoc contrasts were assessed using Tukey's HSD.

2.4 Results

2.4.1. Compartment Coverage

The three compart ments created by MSP were clearly distinguished at both study sites. The M accounted for the largest percentage of total plot area, covering on average 41.9% at the 2012 site and 40.7% at the 2020 site. F represented on average 29.7% and 35% of the area for the 2012 and 2020 sites, respectively (Figure 17). The undisturbed IF covered the remaining 28.4% (2012) and 24.2% (2020) of the plot areas.

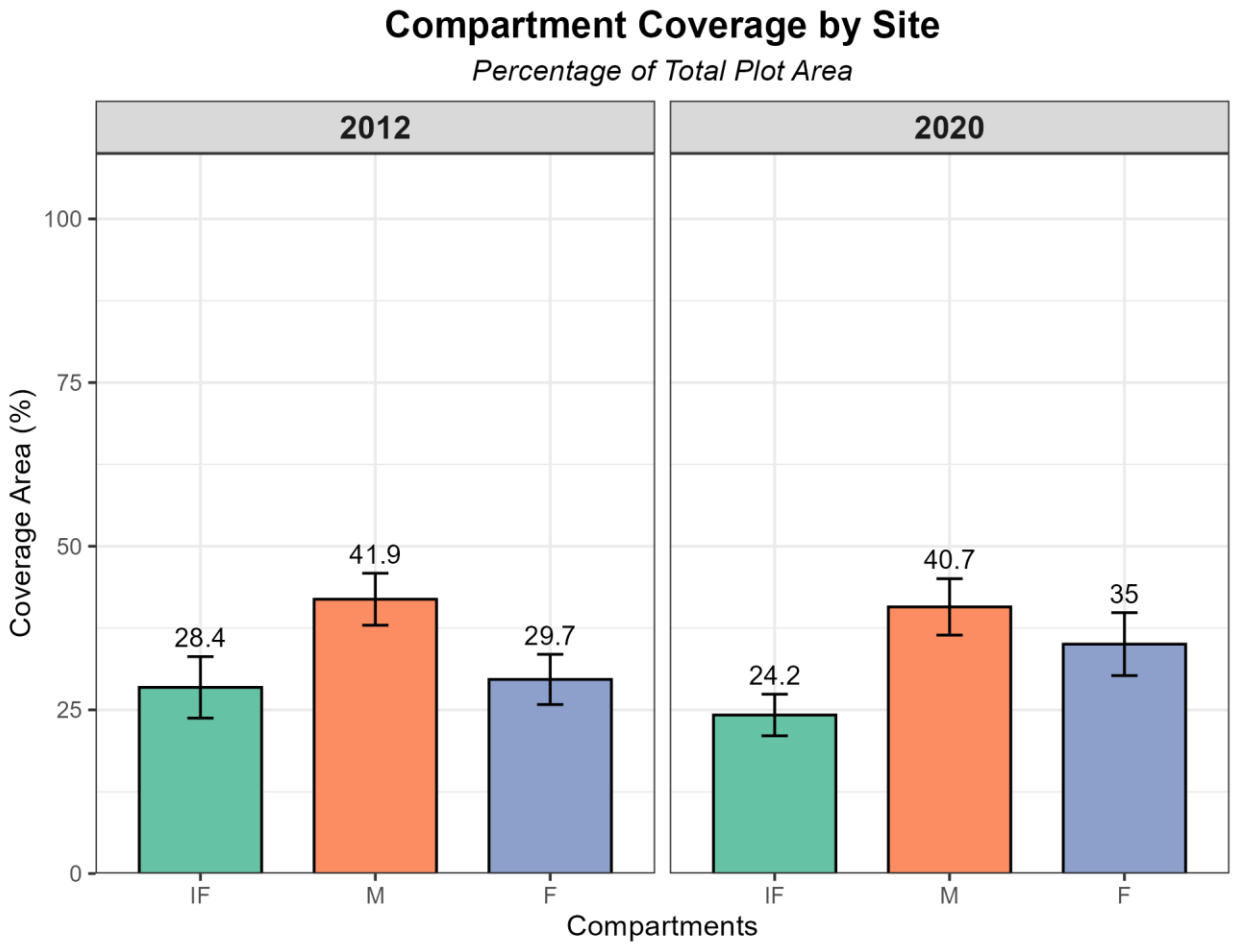

Figure 17: Compartment Area coverage (mean ± SD) in percentage (%) across three compartments: Inter-furrow (IF), Mound (M), and Furrow (F) for the two sites, identified by their year of scarification (2012 and 2020).

2.4.2 Total Carbon Stocks and Carbon Loss

The carbon stocks of the organic horizon in the undisturbed IF compartments were found to be similar across both sites, averaging 8.20 kg C m^{-2} at the 2012 site and 7.40 kg C m^{-2} at the 2020 site (Figure 18). At the 2012 site, the M compartment contained a total of 10.80 kg C m^{-2}. This total was comprised of 10.58 kg C m^{-2} of organic matter divided between the original (5.86 kg C m^{-2}) and the displaced organic layer (4.72 kg C m^{-2}) plus a minor biomass contribution of 0.22 kg C m^{-2}. At the 2020 site, the M compartment contained 13.80 kg C m^{-2}, consisting of 13.67 kg

C m^{-2} of organic matter (7.24 kg C m^{-2} for the original and 6.43 kg C m^{-2} for the displaced layer) plus a biomass contribution of 0.13 kg C m^{-2} (Figure 18). The biomass fraction (above and belowground) in the IF compartment was notably higher at the 2012 site (0.70 kg C m^{-2}) compared to the 2020 site (0.19 kg C m^{-2}). In contrast, the biomass contribution within the M compartment remained negligible at both sites, accounting for only 0.22 kg C m^{-2} at the 2012 site and 0.13 kg C m^{-2} at the 2020 site.

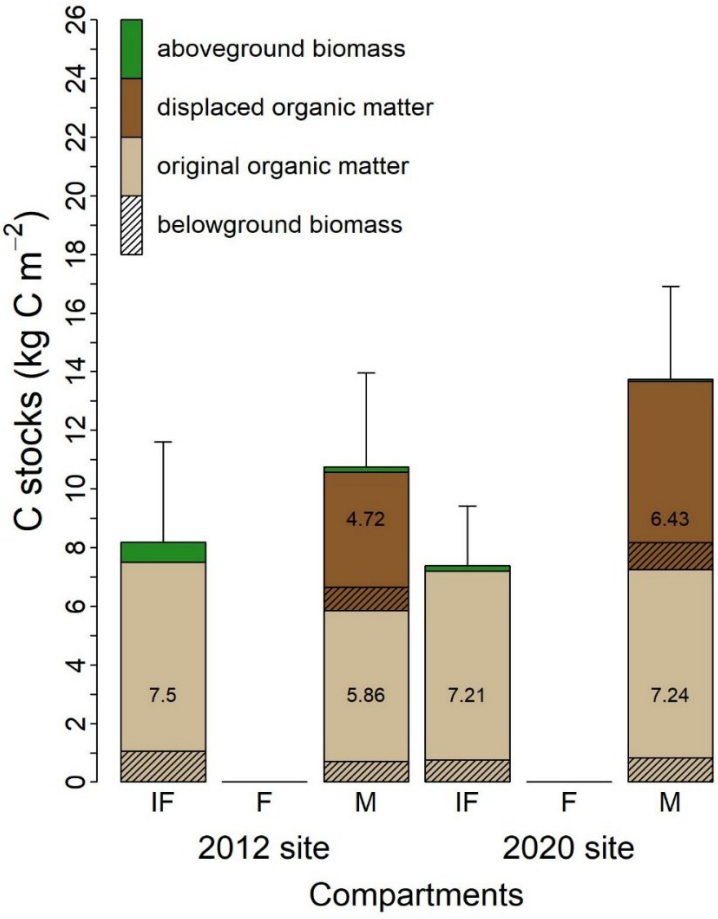

Figure 18: Total carbon stock of the organic horizon in the three compartments (IF: inter-furrow, F: furrow and M: mound) of both sites.

The net impact of MSP on carbon stocks (∆C) varied by site age. The 2012 site exhibited a mean total carbon loss of -0.91 kg C m^{-2} using the method 1, with individual plot values ranging from -3.48 to +1.68 kg C m^{-2} (Figure 19). When method 2 was used, the mean loss was slightly lower at -0.72 kg C m^{-2} (median: -1.13 kg C m^{-2}), with a reduced range of -2.85 to +1.44 kg C m^{-2} (Figure 20). In contrast, no carbon loss was observed at the 2020 site, which showed a mean change of +0.19 kg C m^{-2} (method 1) and +0.02 kg C m^{-2} (method 2), indicating a neutral to slight gain in carbon stocks. Using the method 2, the median change at the 2020 site was -0.51 kg C m^{-2}, though variability was high, ranging from -2.18 to +3.80 kg C m^{-2}. Despite these trends, the difference in total carbon loss between the 2012 and 2020 sites was not statistically significant ($p = 0.31$).

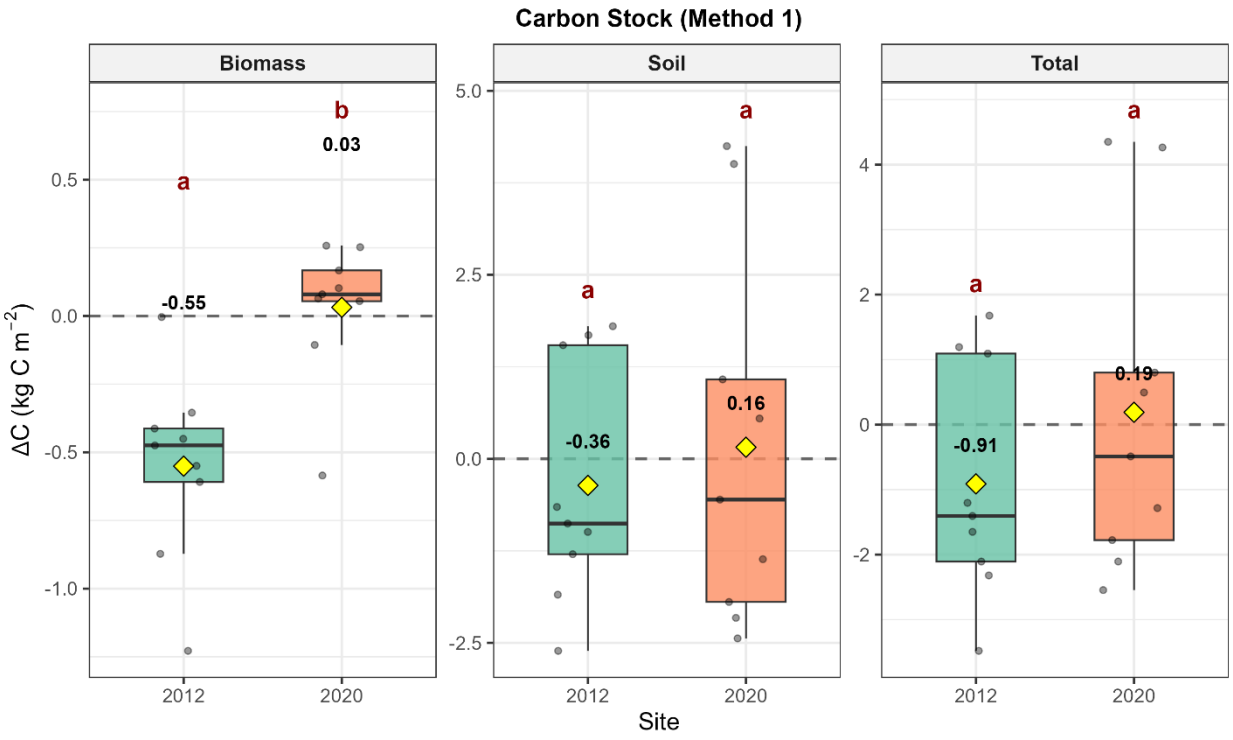

Figure 19: Carbon loss (ΔC; kg C m^{-2}) from biomass, < 2 mm-soil fraction and total organic carbon (biomass + soil) at both sites using method 1. The yellow diamonds represent the mean ΔC value for each site, with the corresponding numerical mean displayed above them. The thick horizontal line within each box indicates the median. Different lowercase letters would indicate statistically significant differences between compartments within the same site ($p < 0.05$); the presence of only the letter 'a' denotes that no significant differences were observed within the biomass, soil and total carbon stock.

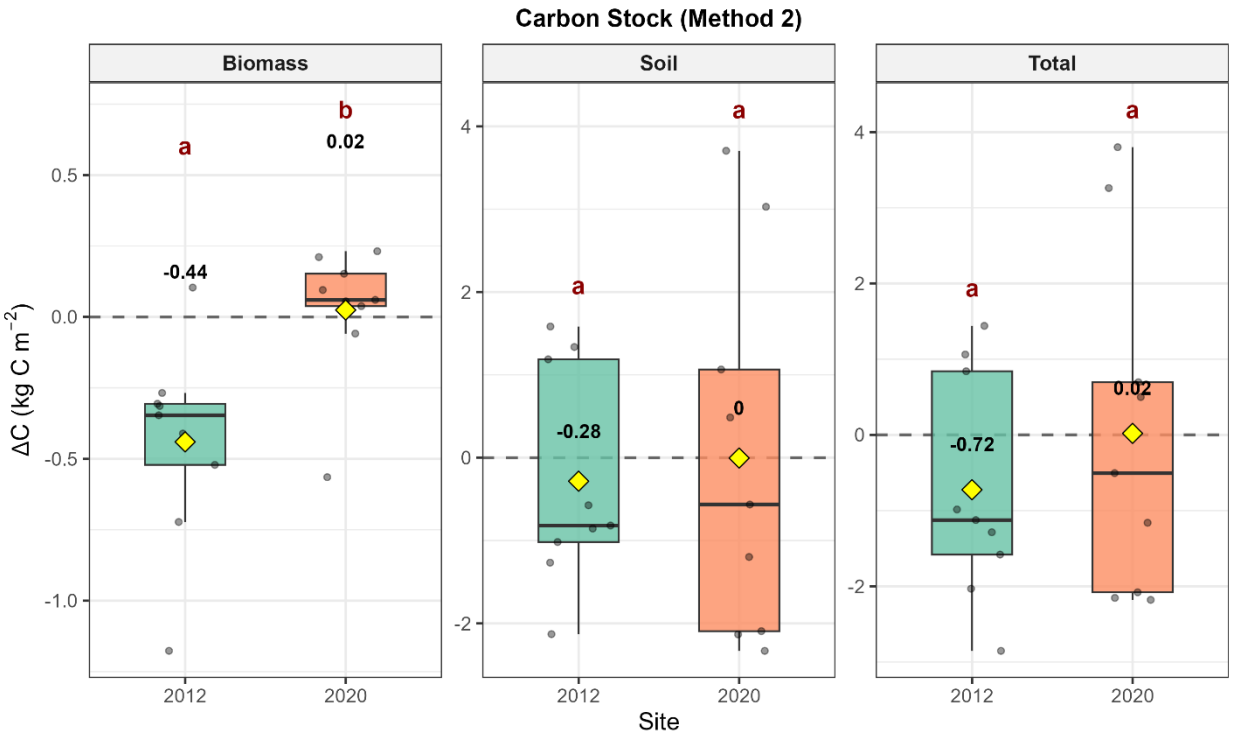

Figure 20: Carbon loss (ΔC; kg C m^{-2}) from biomass, < 2 mm-soil fraction and total organic carbon (biomass + soil) at both sites using method 2. The yellow diamonds represent the mean ΔC value for each site, with the corresponding numerical mean displayed above them. The thick horizontal line within each box indicates the median. Different lowercase letters would indicate statistically significant differences between compartments within the same site ($p < 0.05$); the presence of only the letter 'a' denotes that no significant differences were observed within the biomass, soil and total carbon stock.

2.4.3 Carbon Concentration and C:N Ratios

2.4.3.1 Soil Carbon Concentration

The carbon concentration of the organic horizons exhibited a significant site-dependent response to MSP (Site × Compartment interaction: $F_{2,48} = 5.05$; $p = 0.01$) (Figure 21). While the main effect of compartment (comparing the displaced mound (M_d), original mound (M_{or}), and IF) was not significant when averaged across sites ($p = 0.35$), the interaction reveals distinct trajectories for the two sites (Table 1). At the 2012 site, the displaced M exhibited a significant reduction in carbon

concentration compared to the undisturbed IF. The mean concentration in the displaced M dropped to 17.8%, which was significantly lower than both the undisturbed IF (32.5%; P = 0.01) and the original M (29.6%; P = 0.047). In contrast, the IF and original M did not differ significantly from each other (P = 0.82). At the 2020 site, no significant differences were observed between compartments (P > 0.05). The displaced M exhibited the highest carbon concentration (39.0%), though this was not statistically different from the IF (34.3%) or original M (32.8%).

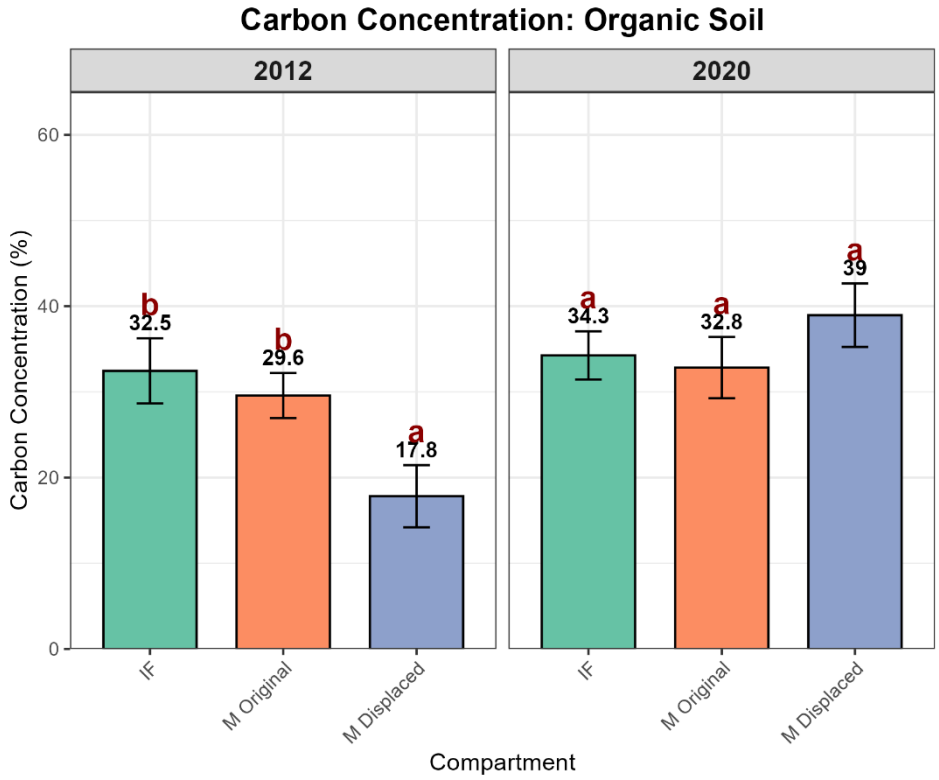

Figure 21: Carbon concentrations (%) in the organic horizons across three compartments: Inter-furrow (IF), original mound (M Original), and displaced mound (M Displaced). Compared between two sites identified by their year of scarification (2012 and 2020). Bars represent the mean carbon concentration, with error bars indicating the standard error of the mean. Numeric values above the error bars denote the specific mean concentration. Different lowercase letters indicate statistically significant differences between compartments within the same site (p < 0.05).

Table 1: Two-way ANOVA results for organic horizon carbon concentration.

Source of Variation	df	F-value	P-value
Site	1	5.79	0.032
Compartment (M_d, M_{or}, IF)	2	0.14	0.716
Site x Compartment	2	5.05	0.010
Residuals	48	-	-

In the mineral horizons (0–15 cm) (Figure 22), no significant differences in carbon concentration were found between compartments ($p = 0.52$) or sites ($p = 0.90$). Although the difference was not significant due to high variability ($F_{2,12} = 0.68$, $P = 0.52$), carbon concentration was about twice higher in F than in IF at the 2012 site.

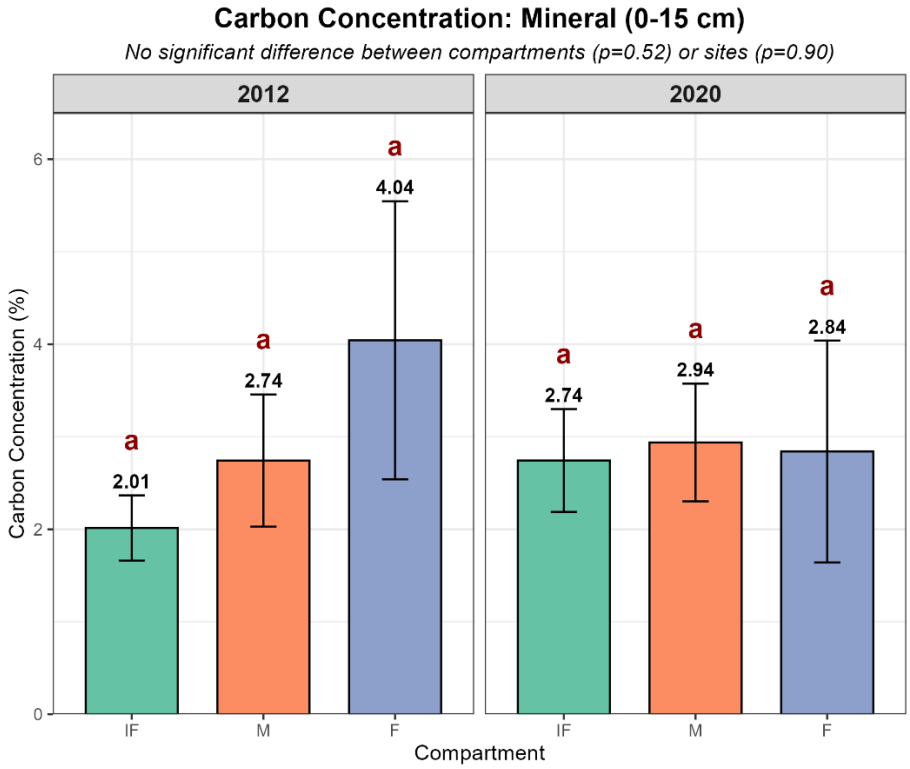

Figure 22: Carbon concentrations (%) in the mineral layer (0–15 cm) across three compartments: Inter-furrow (IF), Mound (M), and Furrow (F) compared between two sites identified by their year of scarification (2012 and 2020). Bars represent the mean carbon concentration, with error bars indicating the standard error of the mean. Numeric values above the error bars denote the specific mean concentration. Different lowercase letters would indicate statistically significant differences between compartments within the same site ($p < 0.05$); the presence of only the letter 'a' denotes that no significant differences were observed within the same site.

2.4.3.2 Soil C:N ratio

In the organic horizons, the C:N ratios followed a similar pattern to carbon concentration (Site × Compartment interaction: $F_{2,48} = 4.03$; $p = 0.02$; Figure 23). At the 2012 site, the displaced M exhibited a significantly lower C:N ratio (average of 18.4) compared to the IF ($p = 0.048$) and the original M ($p = 0.025$) (average of 24.4 and 25.1, respectively). At the 2020 site, C:N ratios remained stable across all compartments ($P > 0.05$), with mean values ranging from 26.2 to 28.4 (Figure 23).

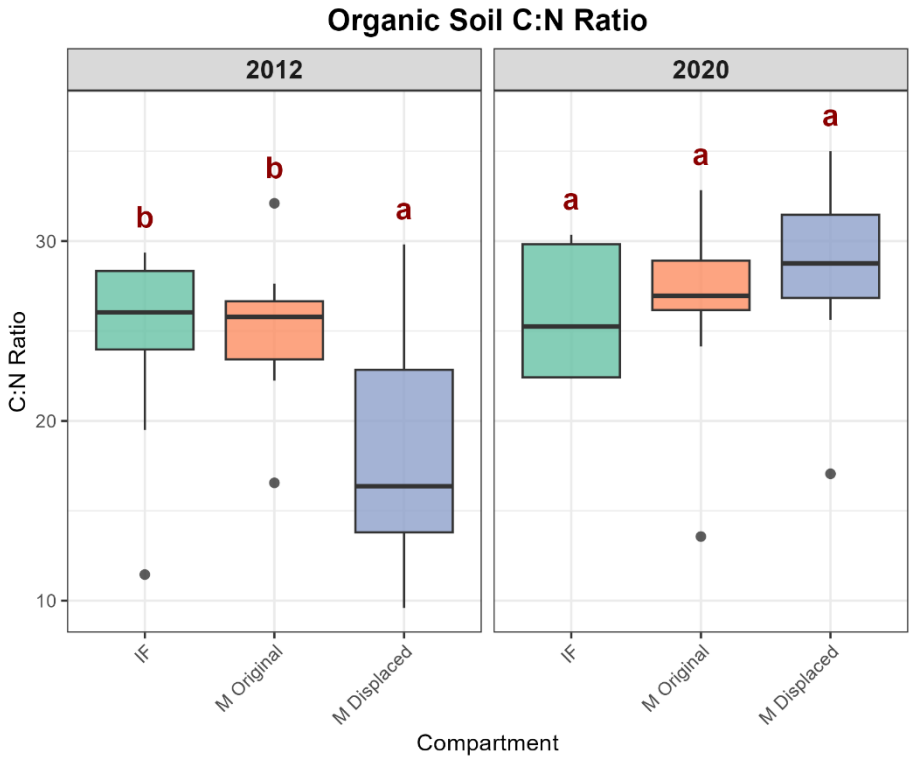

Figure 23: C:N ratios in the organic horizons across three compartments: Inter-furrow (IF), original mound (M Original), and displaced mound (M Displaced) compared between two sites identified by their year of scarification (2012 and 2020). Different lowercase letters indicate statistically significant differences between compartments within the same site ($p < 0.05$); the presence of only the letter 'a' denotes that no significant differences were observed.

In general, the C:N ratio values in the mineral horizons were lower than those observed in the organic layers with mean values lower than 22 across compartments and sites (Figure 24). Statistical analyses indicated no significant effect of Site ($F_{1,12} = 0.07$; $p = 0.80$), Compartment ($F_{2,12} = 1.05$; $p = 0.38$), or their interaction ($F_{2,12} = 0.18$; $p = 0.84$). At the 2012 site, the M and IF compartments showed comparable median C:N ratios (approximately 22 and 21, respectively), while the F compartment displayed a lower median (17) and higher variability. At the 2020 site, the C:N ratio in the M compartment exhibited a median value substantially higher (27) than both

the IF (21) and F (21) compartments, although the difference was not statistically significant (p = 0.41 for M vs. IF and p = 0.72 for M vs. F).

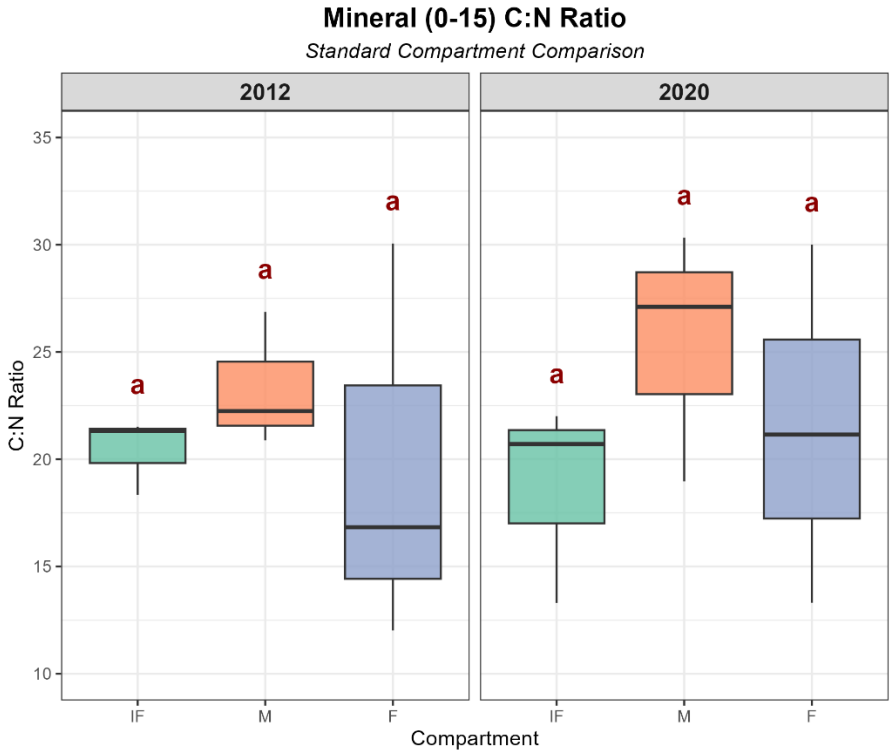

Figure 24: C:N ratios in the mineral layer (0–15 cm) across three compartments: Inter-furrow (IF), Mound (M), and Furrow (F) compared between two sites identified by their year of scarification (2012 and 2020). Different lowercase letters would indicate statistically significant differences between compartments within the same site ($p < 0.05$); the presence of only the letter 'a' denotes that no significant differences were observed.

2.4.4 Soil Organic Matter Separation

2.4.4.1 Mass fractionation

In the organic horizons, the soil mass was dominated by the POM fraction, ranging from 5% to 90% of the organic layer soil mass. A significant interaction was observed between site and compartment for this fraction ($F_{2,46} = 6.17$, $p = 0.004$) (Figure 25), indicating that scarification effects differed by site. At the 2020 site, the M compartment exhibited the highest mean POM fraction (60%) which was higher than

the undisturbed IF (47%), though this difference was not statistically significant ($p = 0.999$). Conversely, at the 2012 site, the POM fraction in the M compartment was significantly lower (15%) than that observed in the undisturbed IF (37%; $p = 0.006$).

In the mineral horizons, both POM and MAOM accounted for a small portion of the total soil mass (< 5% for POM and < 20% for MAOM) (Figure 25), reflecting the dominance of the sand fraction ($F_{1,46} = 30.2$, $p < 0.001$). However, the MAOM fraction constituted a larger proportion of the recovered organic matter compared to POM (averages of 71.5% and 28.5%, respectively).

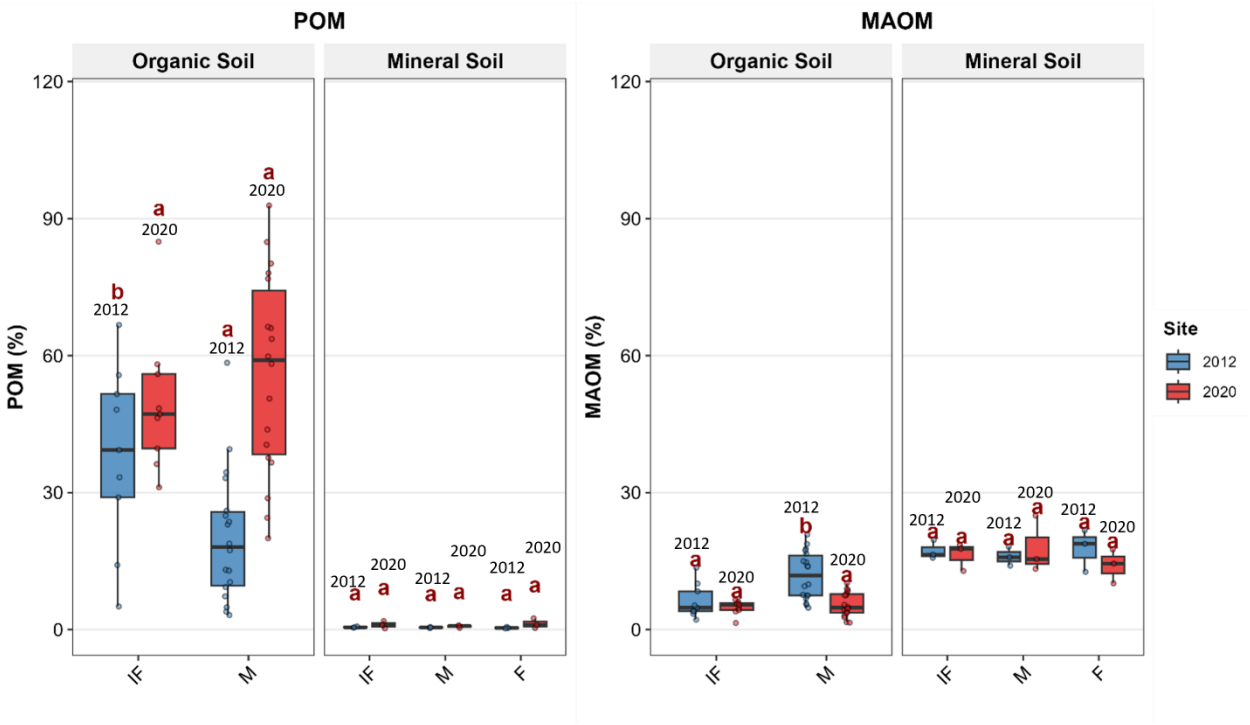

Figure 25: Soil organic matter (SOM) mass fractionation, represented as the mass percentage (%) of particulate (POM) and mineral-associated (MAOM) organic matter. Separated by organic and mineral soil horizons across three compartments: Inter-furrow (IF), Mound (M), and Furrow (F), and compared between two sites identified by their year of scarification (2012 and 2020). Different lowercase letters indicate statistically significant differences between compartments within the same site and soil horizons ($p < 0.05$); the presence of only the letter 'a' denotes that no significant differences were observed.

2.4.4.2 Carbon Distribution between Fractions

In the organic layer soil, the carbon pool was primarily stored within the POM fraction, which accounted for approximately 85–95% of the total carbon across compartments and sites (Figure 26). At the 2012 site, POM accounted for nearly 95% of SOC in the IF compartment, whereas the M compartment showed a higher proportion of carbon associated with the MAOM fraction (15%). At the 2020 site, the carbon distribution was relatively uniform, with POM dominating (>90%) across both M and IF. In the mineral layer soil, the carbon was predominantly associated with

the MAOM fraction. Across all sites and compartments, MAOM accounted for 60-80% of SOC, while POM contributed the remaining 20-40%. At the 2020 site, M exhibited the highest proportion of MAOM-carbon (~80%) compared to the IF (~65%) although the difference was not statistically significant ($F_{2,6}$ = 1.03; p = 0.41).

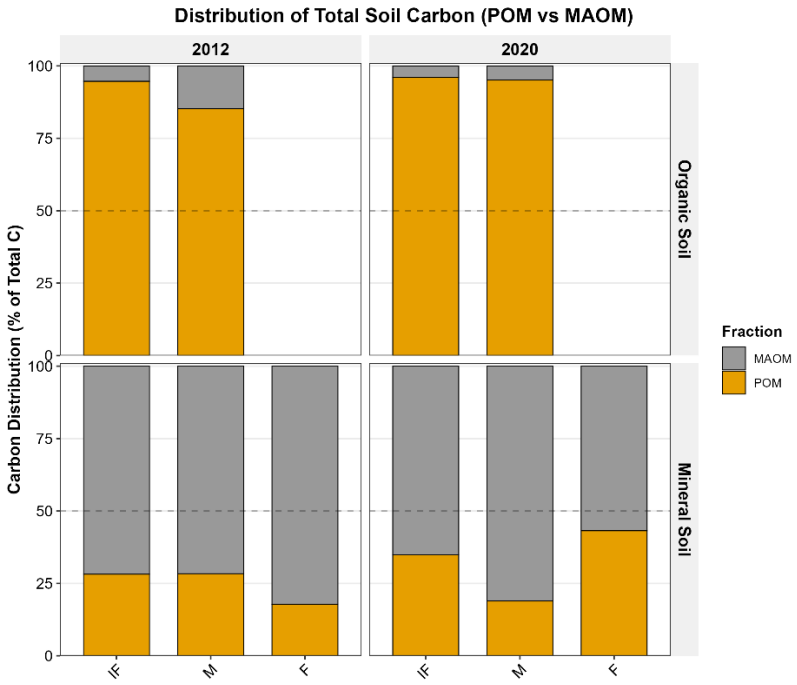

Figure 26: Distribution of Total soil carbon (%) by the three compartments : Inter-furrow (IF), Mound (M) and Furrow (F) at both sites (identified by their year of scarification: 2012 and 2020).

2.4.4.3 C:N Ratio of Fractions

Across all sites and compartments, POM exhibited significantly higher C:N ratios (range of 20–35) compared to MAOM (range of 10–20) (Figure 27). In the mineral layer, the POM fraction in the 2012 site generally exhibited higher C:N ratios (~30) compared to the 2020 site (~25), a difference that was statistically significant (t = 2.36, p = 0.034), which is consistent with the results for bulk soil (Figure 22). When

comparing horizons, two distinct patterns emerged: 1) the C:N ratio of the MAOM fraction was consistently higher in the mineral layer compared to the organic layer soil across all sites and compartments; and 2) the relationship between horizons varied by site. At the 2012 site, POM's C:N ratios were similar between the organic and mineral layer soils, whereas the POM's C:N ratio was slightly higher in the organic layer soil compared to the underlying mineral layer soil at the 2020 site.

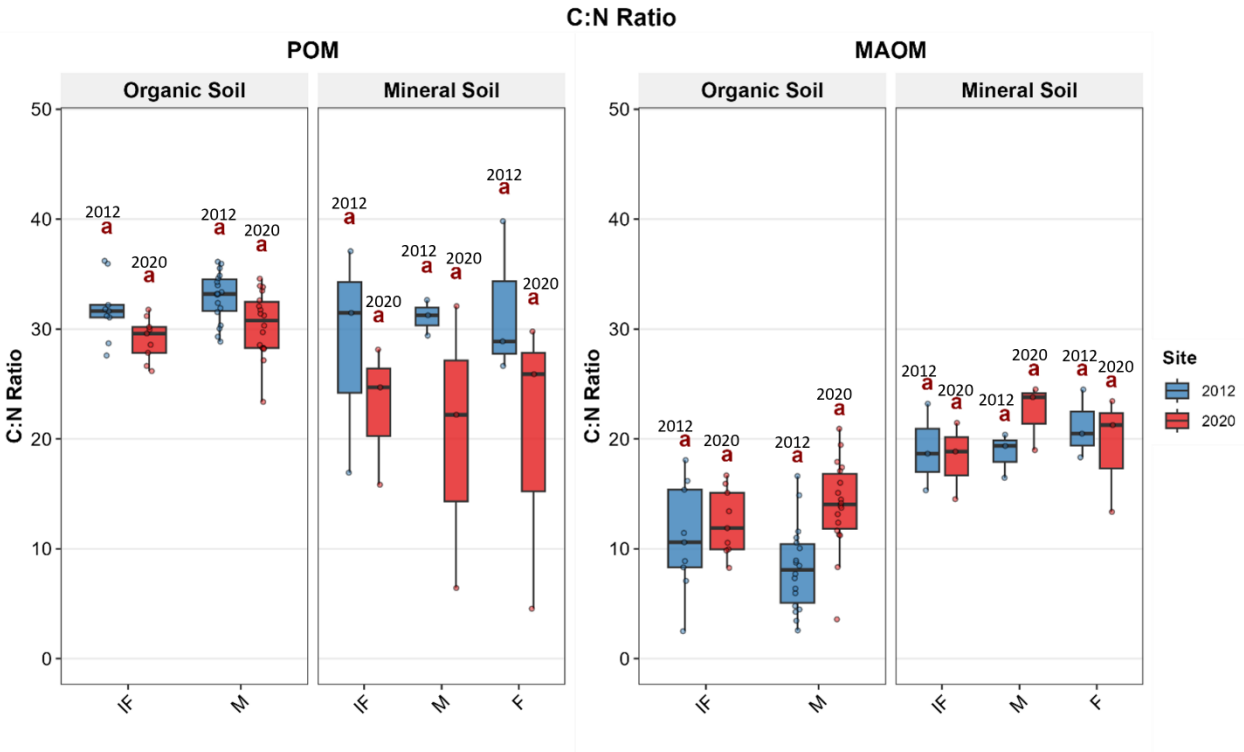

Figure 27: C:N ratios of the particulate (POM) and mineral-associated (MAOM) organic matter fractions in the organic and mineral soil horizons across three compartments: Inter-furrow (IF), Mound (M), and Furrow (F) compared across two sites, identified by their year of scarification (2012 and 2020). Different lowercase letters would indicate statistically significant differences between compartments within the same site between soil horizon ($p < 0.05$); the presence of only the letter 'a' denotes that no significant differences were observed.

2.4.5 Incubation and Temperature Sensitivity (Q_{10})

2.4.5.1 Carbon Mineralization and Respiration Rates

The cumulative CO_2 emissions (C_{cumul}) exhibited a strong exponential increase in response to rising incubation temperatures across all sites, compartments and horizons (Figure 28). In the organic horizons, a significant main effect of compartment was observed on basal respiration (b) ($F_{1,15}$ = 9.55; p = 0.007), independent of site (p = 0.82) (Table 2). The IF consistently exhibited higher b rates compared to the M. Across sites, the mean b for IF was 41.6 ± 9.20 µg CO_2 g^{-1} C, whereas the M averaged significantly lower at 28.4 ± 7.91 µg CO_2 g^{-1} C. In the mineral layer, the respiration dynamics differed. Contrary to the organic layer, no significant difference was found between compartments ($F_{2,14}$ = 0.12; p = 0.89) (Table 3). However, three notable trends were observed. The basal respiration values in the mineral layer soil were high, often exceeding those observed in the organic horizons, with mean values ranging from 38.3 ± 30.5 (F) to 43.7 ± 23.5 (IF) µg CO_2 g^{-1} C. The undisturbed IF compartments displayed markedly lower variability between blocks compared to the disturbed compartments (M and F). A significant site effect was detected ($F_{1,14}$ = 7.26; p = 0.017), with the 2012 site exhibiting significantly higher basal respiration rates compared to the 2020 site. Additionally, Q_{10} in the mineral layer soil differed significantly between sites ($F_{1,12}$ = 10.83; p = 0.006), with the 2020 site exhibiting higher sensitivity (Q_{10} ~ 2.13) compared to the 2012 site (Q_{10} ~ 1.80).

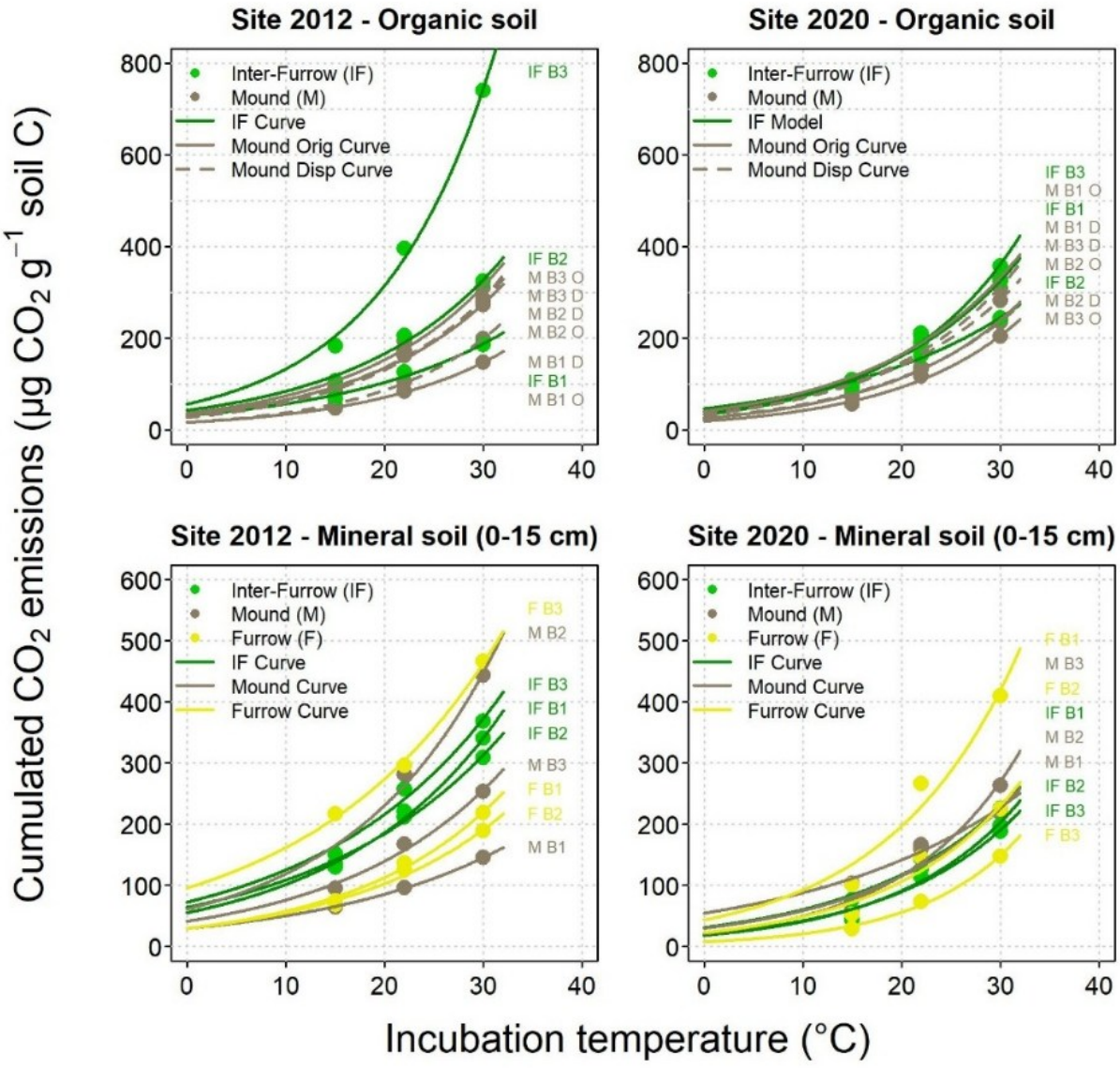

Figure 28: Temperature response curves of cumulative CO_2 emissions (µg CO_2 g^{-1} soil C) for organic (top) and mineral (bottom) horizons. Curves are grouped by compartment Inter-furrow (IF), Mound (M), Furrow (F) and experimental block (B1–B3); for organic M, labels distinguish between original (O) and displaced (D) layers.

Table 2: Basal respiration (b) and temperature sensitivity (Q_{10}) coefficients in the organic and mineral soil horizons across compartments and sites.

Horizon	Site	Compartment	Basal respiration (b) ($\mu g\ CO_2\ g^{-1}$ soil C)	Q_{10}
Organic	2012	Inter-Furrow	43.6 ± 12.5	2.05 ± 0.28
		Mound (Displaced)	25.0 ± 7.84	2.19 ± 0.11
		Mound (Original)	28.4 ± 10.5	2.06 ± 0.02
	2020	Inter-Furrow	39.7 ± 6.64	1.99 ± 0.24
		Mound (Displaced)	31.6 ± 3.99	2.06 ± 0.05
		Mound (Original)	28.5 ± 11.2	2.11 ± 0.10
Mineral	2012	Inter-Furrow	64.2 ± 8.65	1.75 ± 0.07
		Mound	44.2 ± 16.0	1.82 ± 0.12
		Furrow	51.8 ± 38.1	1.83 ± 0.13
	2020	Inter-Furrow	23.2 ± 7.02	2.10 ± 0.14
		Mound	35.4 ± 17.3	1.97 ± 0.36
		Furrow	24.8 ± 17.9	2.32 ± 0.30

Table 3: ANOVA summary for basal respiration (b) and temperature sensitivity (Q_{10}) across organic and mineral horizons.

Horizon	Parameter	Source of Variation	df	F-value	P-value
Organic	b	Site	1	0.04	0.837
		Compartment	2	4.13	0.043
		Site x Compartment	2	0.49	0.625
		Residuals	12	-	-
	Q_{10}	Site	1	0.38	0.550
		Compartment	2	0.76	0.491
		Site x Compartment	2	0.56	0.588
		Residuals	10	-	-
Mineral	b	Site	1	7.21	0.020
		Compartment	2	0.12	0.892
		Site x Compartment	2	0.95	0.413
		Residuals	12	-	-
	Q_{10}	Site	1	10.89	0.008
		Compartment	2	1.31	0.312
		Site x Compartment	2	1.03	0.391
		Residuals	10	-	-

A significant negative linear relationship was observed between substrate lability (represented by basal rate b) and temperature sensitivity (Q_{10}) in the mineral layer only ($p < 0.05$) (Figure 29). Samples with low basal respiration (indicating recalcitrant carbon) exhibited high Q_{10} values, meaning their decomposition is more sensitive to

warming. Conversely, samples with high basal respiration (indicating labile carbon) had lower Q_{10} values. This constraint explains the differences observed between the sites. The 2020 site clustered toward the left/top of the graph, characterized by lower basal rates but significantly higher temperature sensitivity (p = 0.008). In contrast, the 2012 site clustered toward the right/bottom, exhibiting higher respiration but lower sensitivity to temperature.

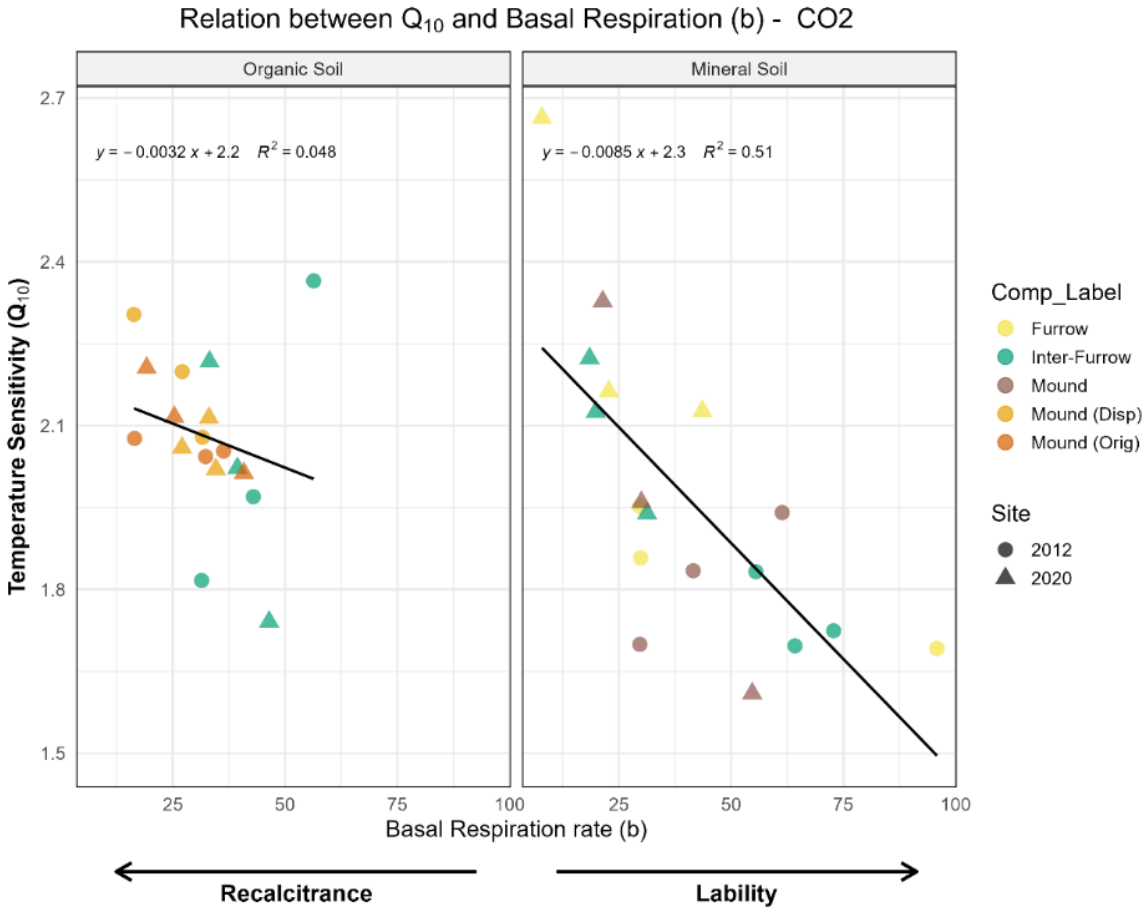

Figure 29: Relationship between soil respiration's temperature sensitivity (Q_{10}) and basal respiration (b) across sites and compartments for organic and mineral soil horizons.

2.4.5.2 Nitrogen and Phosphorus Mineralization

Nitrogen mineralization (NH_4 production) was highly variable across sites and compartments (Figure 30). Unlike carbon respiration, nitrogen dynamics showed no consistent exponential response to temperature, with most compartments exhibiting net immobilization (negative rates) across the incubation range (15–30°C). In the organic horizons, rates were consistently negative regardless of the disturbance, indicating strong N-immobilization. A significant main effect of compartment was observed ($F_{1,40} = 65.4$; $p < 0.001$). Immobilization rates were about two-fold higher in the undisturbed IF (mean of -139 ± 37 μg N g^{-1} h^{-1}) compared to the M (mean of -73.0 ± 34 μg N g^{-1} h^{-1}). Additionally, immobilization rates between compartments were significantly influenced by temperature ($F_{2,40} = 3.68$; $p = 0.034$), with a significant Compartment × Temperature interaction ($F_{2,40} = 4.89$; $p = 0.013$) reflecting a higher temperature response in IF than in M (Figure 28). In the mineral layer (0-15 cm), significant main effects of compartment ($F_{2,34} = 5.48$; $p = 0.009$) and temperature ($F_{2,34} = 5.38$; $p = 0.009$) were detected, but no site effect ($p = 0.73$). However, a significant Site × Temperature interaction ($F_{2,34} = 7.86$; $p = 0.002$), reflecting a lower increase in NH_4 immobilization with increasing temperature at the 2012 site and the unique pattern observed in the F compartment at the 2012 site, which exhibited a distinct shift toward net mineralization at higher temperatures (22°C and 30°C), while the IF and M compartments remained in a state of net immobilization.

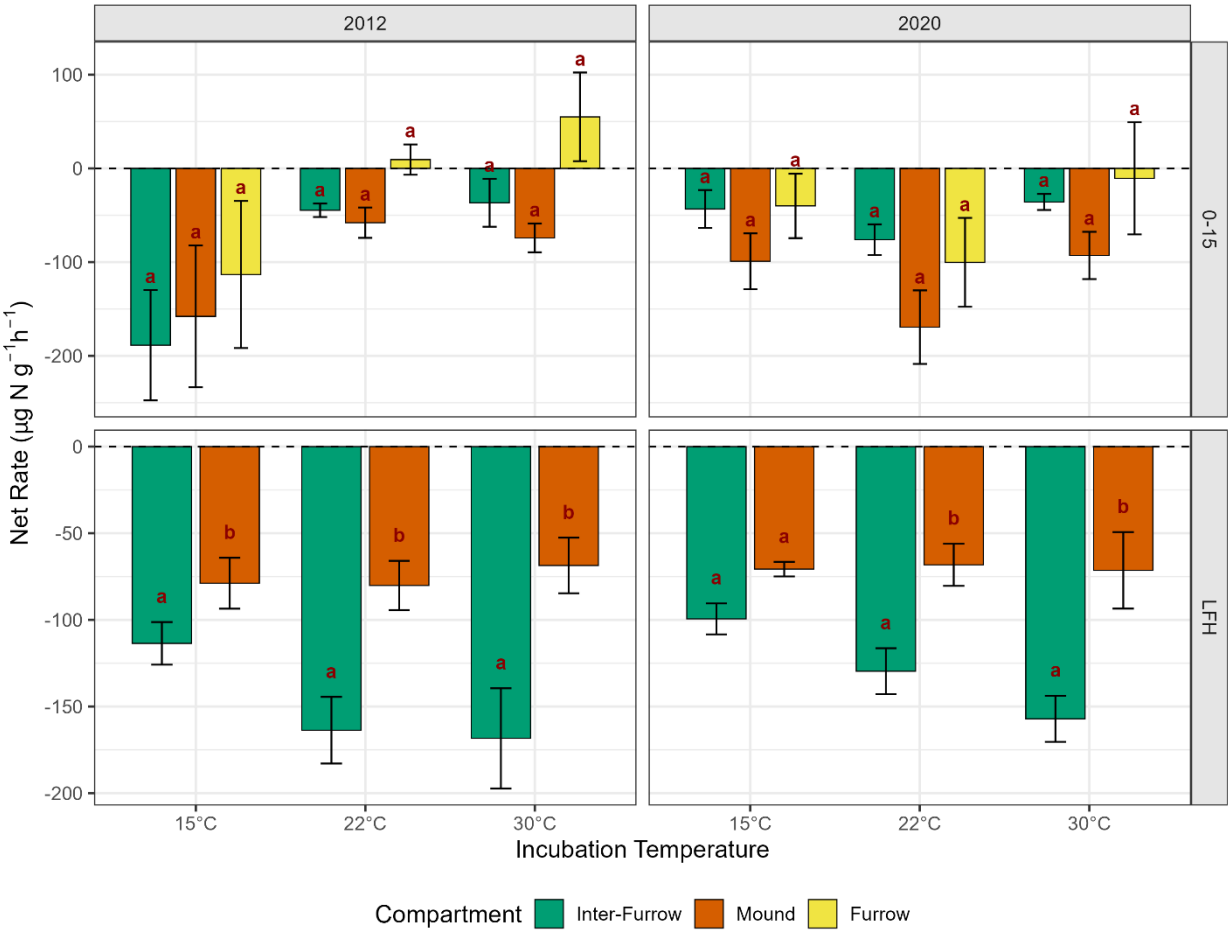

Figure 30: Net rate (µg N g^{-1} h^{-1}) of nitrogen mineralization with incubation temperature of organic and mineral soil horizons across compartments and both sites (identified by their year of scarification: 2012 and 2020). Error bars represent the standard error of the mean. Different lowercase letters indicate statistically significant differences between compartments within the same incubation temperature ($p < 0.05$).

Phosphorus (PO_4) mineralization data is reported exclusively for the organic horizons because analysis of the mineral layer (0–15 cm) yielded concentrations below the detection limit. In the organic horizons (Figure 31), phosphorus dynamics were characterized by net immobilization (negative net rates) across all samples. This indicates that available phosphorus was depleted, likely driven by a combination of high microbial biological demand (microbial immobilization) and

potential geochemical sorption processes within the disturbed organic layer. Unlike carbon, temperature had no significant effect on phosphate mineralization rates ($F_{2,50}$ = 1.22; P = 0.30), with values remaining consistently negative from 15°C to 30°C. A significant compartment effect was observed at the 2012 site ($F_{1,50}$ = 5.16; P = 0.028). The undisturbed IF soils exhibited the highest rates of immobilization, with a mean rate of -1.30 ± 0.90 µg P g^{-1} h^{-1}. In comparison, the M soils showed significantly lower immobilization rates, averaging -0.52 ± 0.36 µg P g^{-1} h^{-1}.

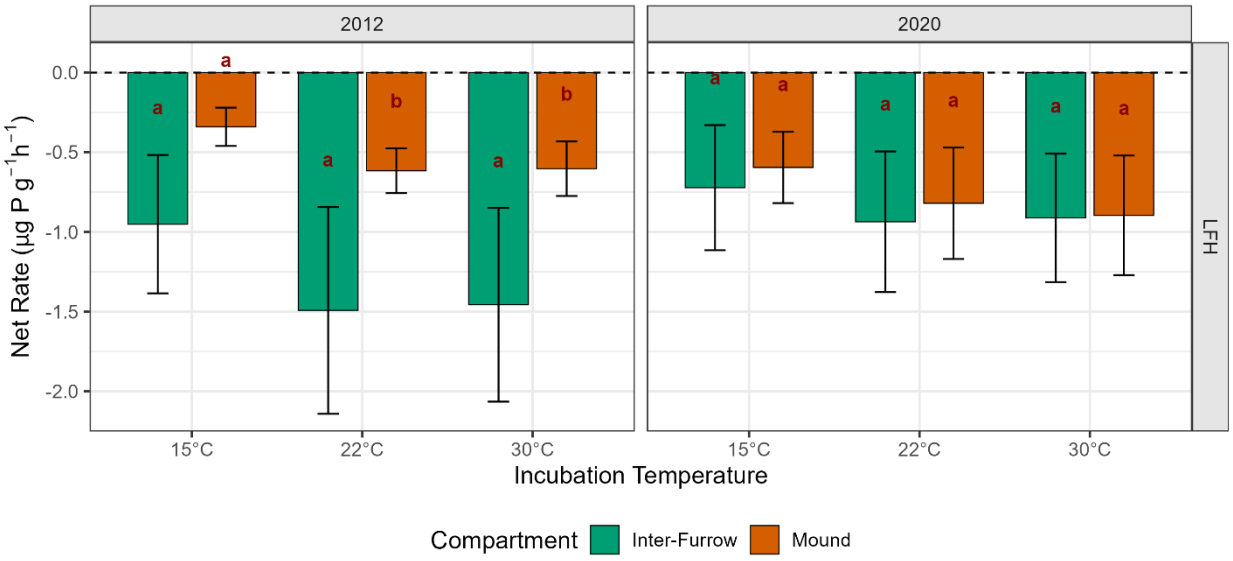

Figure 31: Net rate (µg N g^{-1} h^{-1}) of phosphorus mineralization with incubation temperature of organic layer across compartments and both sites (identified by their year of scarification: 2012 and 2020). Error bars represent the standard error of the mean. Different lowercase letters indicate statistically significant differences between compartments within the same incubation temperature ($p < 0.05$).

2.4.6 Dissolved Organic Carbon (DOC)

Analysis of DOC concentrations indicated significant main effects of compartment ($F_{1,17}$ = 23.51, $p < 0.001$) and horizon ($F_{2,17}$ = 5.58, p = 0.014) (Figure 32). At the 2012 site, vertical stratification was not statistically significant within either the M or IF compartments ($p > 0.05$). Following the removal of the outlier in the M_{or} layer,

DOC concentrations in the mineral layer (0–15 cm) were statistically comparable to those in the overlying organic horizons. In contrast, the 2020 site exhibited significant vertical and compartment-specific differences. Within the M compartment, a significant vertical gradient was observed ($p = 0.016$); DOC concentrations were highest in the surface M_d horizon (31.68 ± 3.52 mg L^{-1}) compared to the buried M_{or} horizon (16.13 ± 3.52 mg L^{-1}). Additionally, DOC concentrations in the 0–15 cm mineral layer was significantly higher in the M than in the undisturbed IF compartment ($p = 0.001$).

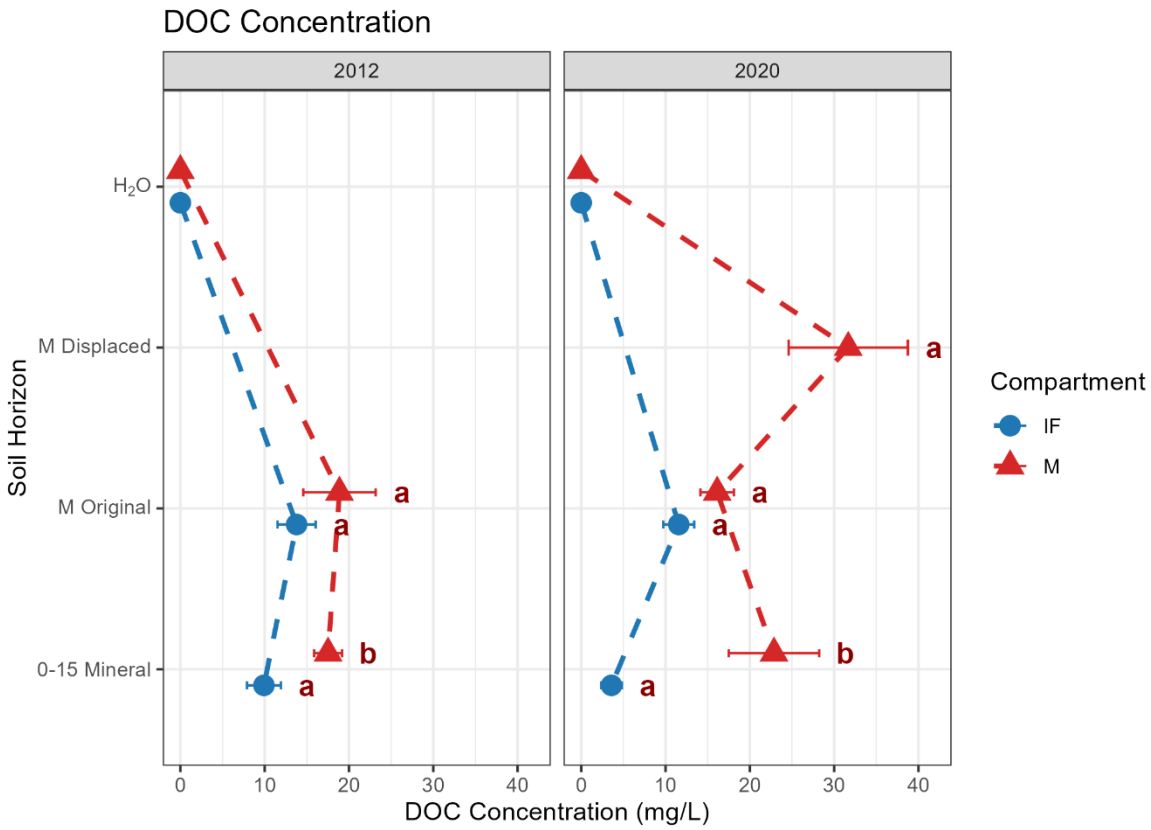

Figure 32: Dissolved organic carbon (DOC) concentrations (mg L^{-1}) across soil horizons at both sites with incubation temperature of organic and mineral soil horizons across compartments (Inter-Furrow (IF), Mound (M)) and sites (identified by their year of scarification: 2012 and 2020). Dashed lines illustrate the vertical change in concentration as water percolates downward from the initial water input (H_2O blank) through the successive physical soil layers. The Y-axis is ordered spatially from the top of the leaching column down to the underlying mineral layer, reflecting the vertical flow of the leachate.

2.5. Discussion

2.5.1. SOC debt is driven by POM loss

Our results suggest that the impact of MSP on SOC storage in LWs varies significantly over time, ultimately resulting in a substantial carbon debt. At the older (2012) site, we observed a mean carbon loss ranging from 7.2 to 9.1 t C ha^{-1} (0.72 to 0.91 kg C m^{-2}), representing approximately 9–11% of the initial organic horizon carbon stock (assuming an average IF baseline of ~8.0 kg C m^{-2}, comparable to the

organic horizon stocks of 4.2–6.5 kg C m^{-2} reported by Marty et al., 2024). Method 1, which assumes widespread degradation beneath the entire mound footprint, likely overestimates this loss, whereas Method 2 provides a more conservative bound by assuming only the central core heavily disrupts the buried organic layer. Regardless of the calculation method, these findings challenge the assumption that scarification merely redistributes soil carbon across the landscape; rather, it may demonstrate that a substantial portion is actively lost from the system (Jandl et al., 2007). Our observed losses are higher than the 2 t C ha^{-1} debt reported by Dufour et al. (2024) in Quebec LWs and the 3–4 t C ha^{-1} deficit assumed in regional carbon budget models (Gaboury et al., 2009; Mansuy et al., 2013), and they contrast with the long-term stability of SOC stocks reported by Strömgren et al. (2026) in hemiboreal trials. However, they align closely with studies observing rapid declines following MSP (Aoyama et al., 2011) and the 5-15 t C ha^{-1} debt commonly reported in closed-canopy boreal forests (Jandl et al., 2007; Johansson, 1994).

This significant carbon loss is a direct consequence of destabilizing a SOM pool that is fundamentally vulnerable. Our fractionation results reveal that the organic layer is overwhelmingly dominated by POM, consisting largely of partially decomposed lichen thalli, spruce needles, and ericaceous leaves. Unlike MAOM, POM is not physically protected by chemical bonds to mineral surfaces and is therefore more vulnerable to biological decomposition and physical alteration (Lavallee et al., 2020). In undisturbed LWs, this dead organic matter accumulates simply because cold temperatures and a lack of soil mixing constrain biological activity. However, once MSP disrupts the physical integrity of the forest floor, this "unprotected" POM

becomes highly vulnerable to microbial consumers and physical erosion (Jandl et al., 2007; Mayer et al., 2020). The active biological decomposition of this fraction at the 2012 site is evidenced by a lower bulk C:N ratio in the displaced M than in the IF compartment, indicating advanced microbial decomposition. Concurrently, the significant reduction in overall POM percentage within this compartment points to the physical loss of a part of this unprotected material likely through aeolian and hydraulic erosion. Interestingly, while the bulk soil C:N ratio declined, the C:N ratio of the isolated POM fraction itself remained relatively stable. This stability suggests that the POM is not simply undergoing partial, gradual chemical alteration in place; rather, once a POM particle becomes accessible, it is either rapidly mineralized by decomposers or physically removed from the system, leaving the remaining intact particulate matter chemically consistent with its original state.

2.5.2. Stability of mineral layer soil carbon

Despite the carbon debt observed in the organic horizon, our results showed no significant decline in total organic carbon concentrations of mineral layer among compartments following disturbance (Figure 22; Table 3). The consistently low C:N ratios observed in the MAOM fraction (ranging from 10 to 20) compared to the POM fraction (20–35) indicate that this organic carbon of mineral layer is highly processed, consisting primarily of microbial necromass and metabolic byproducts (Cotrufo et al., 2015; Lavallee et al., 2020). Historically, this fraction was viewed as a strictly passive and inert vault (Trumbore & Harden, 1997). However, our incubations showed that basal respiration in the undisturbed IF mineral horizon was high under controlled laboratory conditions, in some cases exceeding that of the

organic horizons (e.g., 64.2 ± 8.65 μg CO_2 g^{-1} h^{-1} in the 2012 IF mineral layer vs. 43.6 ± 12.5 μg CO_2 g^{-1} h^{-1} in the organic layer).

This high *in vitro* respiration indicates a highly capable microbial community that can rapidly turn over this mineral-associated carbon—likely reflecting the rapid mineralization of the smaller, unprotected POM fraction and DOC—once environmental bottlenecks are removed. This aligns with perspectives that deep mineral layer organic carbon, while older, is not intrinsically more recalcitrant, but rather its turnover is sensitive to environmental conditions and fresh carbon inputs (Fontaine et al., 2007; Rumpel & Kögel-Knabner, 2011). Yet, the apparent stability of this pool in the field is primarily driven by two factors. First, the chemical bonding of MAOM to silt and clay particles provides a degree of protection against the short-term physical shock of MSP (Mayer et al., 2020), and the absolute carbon concentration in the mineral layer is intrinsically low, limiting the total pool of vulnerable substrate. Second, *in situ* field conditions in LWs—characterized by suboptimal temperatures and restrictive moisture regimes—severely constrain biological activity. Therefore, while the mineral microbial community is highly capable of respiration when optimized in the laboratory, harsh field conditions act as the primary barrier, preserving the mineral carbon stocks even after the overlying forest floor is disturbed.

2.5.3. Temporal Dynamics of Disturbed Organic Matter

While the ultimate loss of carbon is severe, the contrasting carbon balances between the 2012 and 2020 sites suggest that these losses do not occur over the short term upon disturbance. At the recently scarified 2020 site, the M compartment retained

high carbon concentrations and C:N ratios similar to the undisturbed IF. Using the conservative Method 2, the 2020 site exhibited a negligible 0.2 t C ha^{-1} change, reflecting essentially no net loss across the landscape immediately following MSP.

This short-term stability aligns with the concept of a "decomposition lag" (Bradford et al., 2016; Prescott, 2010). Because carbon storage in the organic layer relies primarily on the physical, structural integrity of the POM rather than chemical mineral associations, it takes time for this structural litter to break down. Following the initial fragmentation of the lichen mat and ericaceous shrub layer, microbial communities require a lag period to fully colonize the disrupted substrate, adapt to the altered pedoclimatic conditions, and reach peak mineralization rates (Bradford et al., 2016; Prescott, 2010; Strömgren et al., 2017). This delayed response is consistent with observations in other disturbed forest soils, where peak heterotrophic respiration and measurable carbon depletion only manifest several years after the initial scarification event (Aoyama et al., 2011; Kataja-aho et al., 2012). The high concentration of POM in the M compartment at the 2020 site further highlights this lag, representing an accumulation of translocated surface litter that has not yet decomposed. The 2012 site, having passed this lag phase, clearly demonstrates the breaking point where the physical structure fails and rapid carbon depletion ensues.

2.5.4. Impact on Soil Fertility and Ecosystem Regeneration

The ultimate ecological consequence of this carbon loss might be a severe disruption of microbial metabolic activity and nutrient availability, directly impacting the regenerating trees. In undisturbed IF soils, high basal respiration is maintained by the "rhizosphere priming effect" (Kuzyakov, 2010), where intact root-mycorrhizal

networks supply a steady stream of fresh exudates and litter (Högberg et al., 2001). Scarification severs these networks (Hannam et al., 2006). After the initial post-disturbance flush of labile carbon is consumed, the microbial community enters a state of severe carbon limitation. Consequently, basal respiration in the displaced M dropped by 20% relative to the IF at the 2020 site and plummeted by over 40% at the older 2012 site.

This biological exhaustion leaves behind a more recalcitrant organic residue, evidenced by the significant narrowing of the C:N ratio in the 2012 M (~18–20) compared to the IF (~26). Decomposers selectively mine the most labile substrates, retaining nitrogen to meet strict stoichiometric demands while respiring carbon (Cotrufo et al., 2013; Craine et al., 2015; Marty et al., 2011; Schimel & Bennett, 2004). The Q_{10} of SOM decomposition ranged between 1.75 ± 0.07 and 2.32 ± 0.30 across all sites and compartments. These values are consistent with the global average for forest soils and align closely with previous findings for boreal ecosystems (Laganière et al., 2012), including the Q_{10} values reported by Marty et al. (2019) in their study of similar regional soils. Notably, there was no drastic shift in Q_{10} between the disturbed M and undisturbed IF organic layers (e.g., 2.19 ± 0.11 vs. 2.05 ± 0.28 at the 2012 site). This indicates that while scarification reduced the total pool of labile carbon, thus lowering the basal respiration capacity, it did not fundamentally alter the thermodynamic nature of decomposition.

Crucially, our results revealed widespread net nitrogen and phosphorus immobilization across the organic horizons, a dynamic that reflects the inherent baseline conditions of these ecosystems rather than a consequence of disturbance.

In fact, nutrient immobilization tended to be higher in the undisturbed IF compartment. Because the natural substrate C:N ratio in LWs (>25:1) inherently exceeds the critical threshold for microbial growth, microbes must continuously scavenge mineral N to maintain their biomass (Craine et al., 2007; Mooshammer et al., 2014; Schimel & Weintraub, 2003). While laboratory incubations showed the heavily processed MAOM in the mineral F can theoretically mineralize N under extreme 30°C conditions (Booth et al., 2005; Fontaine et al., 2007; Rumpel & Kögel-Knabner, 2011; Trumbore & Harden, 1997), restrictive *in situ* temperatures ensure immobilization remains the dominant field reality.

Ultimately, this biological lock-up may partly explain the slow growth rates of trees even after scarification. While the artificial M provides a physically favorable planting site and successfully reduces vegetative competition (Hébert et al., 2006; Prévost, 1997), it does not alleviate the fundamental nutrient deficiency of the soil. Establishing seedlings are still forced to compete with the microbial community for limited available nutrients (Craine et al., 2015; Kaye & Hart, 1997).

2.5.5. Disentangling physical from biological mechanisms

The massive reduction in carbon concentration within the displaced M at the 2012 site —dropping to 17.8% compared to 32.5% in the undisturbed IF— is a product of distinct physical and biological mechanisms. While Marty et al. (2024) observed a similar ~25% decline, understanding the true fate of this carbon requires disentangling physical dilution from active loss.

The majority of this concentration drop was shown to be a physical artifact of the scarification machinery, as intensive mounding mixes carbon-depleted mineral layer from the F into the carbon-rich organic M (Marty et al., 2024; Nordborg et al., 2003). Specifically, the displaced M at the 2012 site contained an average of 67.9% sand, compared to 55.7% in the undisturbed IF organic layer and 82.2% in the underlying mineral layer. Assuming an average carbon concentration of 2% for the incorporated mineral layer, this mixing model indicates that the displaced M is composed of roughly 46% mineral layer, meaning physical dilution alone accounts for approximately 95% of the observed decline in carbon concentration. This mixing is further supported by the increased proportion of MAOM in the 2012 M compartment, as machinery imported pre-existing mineral-bound carbon from below. Because this mineral-associated fraction inherently possesses a significantly lower C:N ratio than the organic POM, its physical incorporation may contribute to the overall narrowing of the bulk C:N ratio observed in the displaced mound.

However, the remaining 5% decline in carbon concentration, alongside the absolute stock loss (7.2–9.1 t C ha^{-1}), is driven by both biological and physical removal mechanisms. Scarification disrupts the equilibrium between litterfall and decomposition; it halts fresh carbon inputs to the soil by removing vegetation while simultaneously stimulating microbial respiration through increased soil aeration and temperature (Burgess et al., 1995; Jandl et al., 2007; Kataja-aho et al., 2012; Mallik & Hu, 1997; Strömgren et al., 2017). Furthermore, the absolute loss of carbon from the M compartment observed at this site is likely also explained by a physical loss of SOM particles through erosion driven by wind and precipitation. This would

explain the large decline in carbon stock despite a limited decline in carbon concentration once dilution is accounted for. Because MAOM is physically protected and heavier, it remains in place, while the lighter, unprotected POM is easily eroded via wind displacement or leaching. As this lighter POM is selectively removed, the POM to MAOM ratio decreases over time, causing the bulk C:N ratio to naturally decline because the remaining MAOM inherently possesses a lower C:N ratio.

Concurrently, a substantial portion of this carbon may be lost through liquid pathways. Forest disturbances are widely documented to alter hydrology and increase DOC leaching (Kalbitz et al., 2000; Piirainen et al., 2002; Smolander et al., 2001). The physical fragmentation of the organic layer results in a flush of soluble carbon leaching downward with infiltrating precipitation (Hannam et al., 2006; Hope, 2007). We observed higher DOC leaching beneath the displaced M compartment compared to the undisturbed IF, with concentrations peaking at 31 mg C L^{-1} at the 2020 site. While the active leaching phase is most pronounced shortly after disturbance, the gradual decline in DOC mobilization at the older 2012 site indicates that the finite pool of highly soluble, readily available carbon generated by the initial scarification has been progressively depleted over time (Kalbitz et al., 2004). Research has shown that a fraction of this mobilized DOC is adsorbed by deep mineral horizons (Kaiser & Guggenberger, 2000; Kothawala et al., 2009), providing a pathway for MAOM formation (Cotrufo et al., 2015; Lavallee et al., 2020) and supporting the hypothesis that not all mobilized carbon is respired to the atmosphere (Marty et al., 2024). However, the exact proportion of the carbon debt lost as gaseous CO_2 versus translocated as DOC remains to be determined. Future

investigations into the carbon dynamics of scarified lichen woodlands should employ continuous water sampling via zero-tension lysimeters to quantify true downward fluxes (Piirainen et al., 2002). Additionally, utilizing stable isotope analyses ($\delta^{13}C$ and $\delta^{15}N$) might also help tracing the origin of the carbon accumulating in the mineral horizons, confirming whether it is newly derived from the buried organic horizons or represents older, pre-disturbance carbon.

2.5.6. Conclusion

Our findings reveal a significant response of SOC dynamics to MSP that appears closely linked to the time elapsed since scarification, though the potential influence of inherent site-level variations must also be considered. The impact on soil carbon stocks evolves gradually following the initial disturbance. While the 2020 site exhibited stable carbon stocks 4 years post-treatment, the 2012 site experienced a substantial net carbon loss from the organic horizon estimated at 7.2-9.1 t C ha^{-1} after 12 years. While the unreplicated nature of the chronosequence (n=1 per age class) warrants caution, the baseline carbon stocks and C:N ratios in the undisturbed IF compartments were remarkably similar across both site 2012 and site 2020. This internal baseline consistency suggests that the contrasting results are largely driven by the time elapsed since scarification rather than purely inherent site-specific differences. However, given the high spatial heterogeneity of boreal ecosystems, sampling a larger, replicated network of sites remains necessary to fully confirm this time-dependent claim. This temporal divergence suggests that the "carbon debt" associated with MSP is not immediate but manifests after a "decomposition lag."

Furthermore, any nascent natural regeneration of vegetation on these 12-year-old M has proven insufficient to offset this substantial carbon loss.

Comparisons among soil compartments elucidate the specific mechanisms driving these long-term changes. At the 2020 site, the displaced organic layer in the M compartment showed no significant decrease in carbon concentration. However, at the older 2012 site, the displaced M exhibited a 15% absolute reduction in carbon concentration (dropping to 17.8%) and a pronounced narrowing of the C:N ratio. As previously established, this drop in concentration is predominantly a physical artifact of dilution—the mechanical incorporation of carbon-depleted mineral layer soil into the organic M layer during MSP. Nevertheless, the narrowing C:N ratio highlights the biological decomposition of the POM fraction—the major fraction of SOC in the organic horizons—once physically disturbed and exposed to aeration. Our incubation results further illustrate this biological shift: the undisturbed IF maintained higher basal respiration rates than the 12-year-old displaced M, likely because the intact IF receives a continuous supply of fresh, labile carbon from living root networks to fuel microbial activity. In the disturbed mounds, the complete cessation of these fresh inputs leads to the progressive exhaustion of their finite labile carbon pool. Consequently, the remaining SOC fraction is more recalcitrant, explaining the lower b values. While physical dilution likely drove a major part of the decrease in carbon concentration in the mounds, the actual loss of 7.2–9.1 t C ha^{-1} was driven by biological and ecological factors and physical displacement of SOC particles through leaching or wind. Furthermore, future investigations should incorporate deeper soil sampling protocols, specifically targeting the mineral Bf horizon, to accurately

quantify the potential downward migration and long-term accumulation of DOC resulting from these leaching processes.

These findings emphasize the critical importance of accounting for the below-ground costs of MSP in nutrient-poor ecosystems. Because LWs are characterized by extremely slow tree growth and minimal annual litter inputs, the recovery period required to "pay back" this carbon debt estimated at 7.2-9.1 t C ha^{-1} at our 12 year-old site, will extend significantly longer than in productive, closed-canopy boreal forests. Therefore, it is imperative to balance the silvicultural benefits of MSP–such as breaking competitive exclusion and exposing mineral layer for seedling establishment–with the reality of medium-term soil carbon depletion. Future forest management strategies in these sensitive ecosystems must consider optimizing the scarification process to minimize the total volume of the displaced organic horizon, ensuring that the eventual carbon sequestration gains from regenerating black spruce are not negated by the extensive destabilization of the soil carbon reservoir

CHAPTER III

GENERAL CONCLUSION

This study advances our understanding of the impacts of mechanical site preparation (MSP) on soil carbon stability in boreal lichen woodlands (LWs). To directly address our core objectives and test the hypothesis that intensive soil disturbance induces a long-term carbon debt, our research provides a comprehensive assessment of how scarification influences carbon stocks, soil organic matter (SOM) fractionation, nutrient dynamics, and the temperature sensitivity (Q_{10}) of soil heterotrophic respiration by comparing site 2020 (4 years post-MSP) and site 2012 (12 years post-MSP).

Our results demonstrate that the impact of MSP on soil carbon appears to be highly dependent on the time elapsed since scarification, though the chronosequence design limits definitive conclusions regarding purely temporal effects. While the 2020 site showed stable total carbon stocks, the 2012 site exhibited a substantial net ecosystem loss of 7.2–9.1 t C ha^{-1} from the organic horizon. As established, the massive reduction in carbon concentration within the disturbed Mounds (M) is overwhelmingly a physical artifact of dilution via the incorporation of carbon-depleted mineral layer during scarification. However, the actual 7.2–9.1 t C ha^{-1} ecosystem stock loss is likely driven by a combination of the biological mineralization and physical erosion of the physically unprotected Particulate Organic Matter (POM) fraction, compounded by a lack of fresh litter inputs. In contrast, the Mineral

Associated Organic Matter (MAOM) pool remained stable, though it was ultimately insufficient to offset the substantial POM losses from the organic horizon. Furthermore, dissolved organic carbon (DOC) analysis revealed that while the displaced M remain a potential source of soluble carbon, this downward flux appears to gradually diminishes over the first decade as the disturbed organic horizon is progressively depleted of its most labile carbon.

We also observed that undisturbed Inter-furrow (IF) soils maintained higher basal respiration than the older M compartments, a finding that adds nuance to the widespread assumption that aeration immediately and continuously stimulates microbial activity. Instead, the severing of the biomass likely interrupts the rhizosphere priming effect, cutting off fresh carbon inputs. Consequently, the disturbed M progressively exhausts their finite pool of labile carbon, inducing a mid-term state of substrate limitation. This confirms that the observed biological carbon debt is driven by a gradual decay following an initial "decomposition lag," rather than an ongoing, continuous respiratory burst.

Despite the valuable insights obtained, several limitations must be acknowledged. First, the use of a chronosequence approach (space for time substitution) relies on the assumption that initial soil conditions were identical across sites prior to disturbance. Because this study utilized a single geographic site per age class (n = 1 for the time factor), it is impossible to entirely decouple temporal progression from inherent, site-specific baseline variations. While site selection was carefully controlled and undisturbed IF conditions were remarkably similar between the two sites, inherent spatial heterogeneity in soil depth and texture may still influence the

calculated carbon stocks. Second, our respiration assessments and Q_{10} values were derived from controlled laboratory incubations. While this allowed for the precise measurement of basal respiration and nutrient mineralization, respiration patterns may be different under field conditions due to the dynamic influence of root exudates, seasonal temperature fluctuations, and freeze-thaw cycles that occur in the field. Third, our DOC measurements represent static concentrations rather than continuous volumetric fluxes, limiting our ability to partition the total carbon loss between gaseous CO_2 emissions and deep mineral stabilization. Finally, our sampling was limited to the organic horizon and the top 15 cm of the mineral horizon. While this captures the most active horizons, it does not account for potential deep-soil carbon dynamics influenced by altered hydrology. Together, these factors suggest that our estimates of carbon loss are conservative and focused primarily on the most vulnerable organic pools.

Future climate projections suggest that rising temperatures could exacerbate the vulnerabilities identified in this study. The finding that remaining recalcitrant organic matter in the M maintains a high intrinsic temperature sensitivity ($Q_{10} \sim 2.0$) implies that as the boreal zone warms, the "decomposition lag" observed could shorten, accelerating the rate of POM mineralization. Furthermore, if climate change prolongs the frost-free season, the annual period of active decomposition for these exposed M will extend, potentially increasing the ultimate magnitude of the carbon debt. Conversely, the eventual establishment of a closed-canopy forest may offset these soil losses through increased litterfall and root inputs, but this recovery is likely to be significantly slower in LWs than in more productive boreal stands.

Therefore, it is imperative to quantify the trade-offs between silvicultural success and soil carbon integrity under current and future management scenarios. Understanding this relationship is crucial to determining whether the carbon sequestered by regenerating black spruce can sufficiently offset the medium-term depletion of the soil carbon reservoir. In this context, optimizing the scarification process to minimize the volume of the displaced organic matter emerges as a key management decision. By shifting towards less intensive scarification methods that preserve the structural and protective functions of the forest floor, forest managers can better align crucial afforestation goals with the global imperative of climate change mitigation.

REFERENCES

Aoyama, K., Yoshida, T., Harada, A., Noguchi, M., Miya, H., & Shibata, H. (2011). Changes in carbon stock following soil scarification of non-wooded stands in Hokkaido, northern Japan. *Journal of Forest Research*, *16*(1), 35-45. https://doi.org/10.1007/s10310-010-0204-y

Benbi, D. K., Boparai, A. K., & Brar, K. (2014). Decomposition of particulate organic matter is more sensitive to temperature than the mineral associated organic matter. *Soil Biology and Biochemistry*, *70*, 183-192. https://doi.org/https://doi.org/10.1016/j.soilbio.2013.12.032

Benbi, D. K., Toor, A. S., & Kumar, S. (2012). Management of organic amendments in rice-wheat cropping system determines the pool where carbon is sequestered. *Plant and Soil*, *360*(1), 145-162. https://doi.org/10.1007/s11104-012-1226-3

Bernier, P. Y., Desjardins, R. L., Karimi-Zindashty, Y., Worth, D., Beaudoin, A., Luo, Y., & Wang, S. (2011). Boreal lichen woodlands: A possible negative feedback to climate change in eastern North America. *Agricultural and Forest Meteorology*, *151*(4), 521-528. https://doi.org/https://doi.org/10.1016/j.agrformet.2010.12.013

Birch, H. F. (1958). The effect of soil drying on humus decomposition and nitrogen availability. *Plant and Soil*, *10*(1), 9-31. https://doi.org/10.1007/BF01343734

Boateng, J. O., Heineman, J. L., McClarnon, J., & Bedford, L. (2006). Twenty year responses of white spruce to mechanical site preparation and early chemical release in the boreal region of northeastern British Columbia. *Canadian Journal of Forest Research*, *36*(10), 2386-2399. https://doi.org/10.1139/x06-197

Booth, M. S., Stark, J. M., & Rastetter, E. (2005). CONTROLS ON NITROGEN CYCLING IN TERRESTRIAL ECOSYSTEMS: A SYNTHETIC ANALYSIS OF LITERATURE DATA. *Ecological Monographs*, *75*(2), 139-157. https://doi.org/https://doi.org/10.1890/04-0988

Bossio, D. A., Cook-Patton, S. C., Ellis, P. W., Fargione, J., Sanderman, J., Smith, P., Wood, S., Zomer, R. J., von Unger, M., Emmer, I. M., & Griscom, B. W. (2020). The role of soil carbon in natural climate solutions. *Nature Sustainability*, *3*(5), 391-398. https://doi.org/10.1038/s41893-020-0491-z

Botroh, A.-M., Paré, D., Cavard, X., Fenton, N., Valeria, O., Marchand, P., & Bergeron, Y. (2023). Nine-years effect of harvesting and mechanical site preparation on bryophyte decomposition and carbon stocks in a boreal forested peatland. *Forest Ecology and Management*, *540*, 121020. https://doi.org/https://doi.org/10.1016/j.foreco.2023.121020

Boucher, J. F., Tremblay, P., Gaboury, S., & Villeneuve, C. (2012). Can boreal afforestation help offset incompressible GHG emissions from Canadian industries? *Process Safety and Environmental Protection*, *90*(6), 459-466. https://doi.org/https://doi.org/10.1016/j.psep.2012.10.011

Bradford, M. A., Wieder, W. R., Bonan, G. B., Fierer, N., Raymond, P. A., & Crowther, T. W. (2016). Managing uncertainty in soil carbon feedbacks to climate

change. *Nature Climate Change*, *6*(8), 751-758. https://doi.org/10.1038/nclimate3071

Bradshaw, C. J. A., Warkentin, I. G., & Sodhi, N. S. (2009). Urgent preservation of boreal carbon stocks and biodiversity. *Trends in Ecology & Evolution*, *24*(10), 541-548. https://doi.org/10.1016/j.tree.2009.03.019

Brady, R. R. W. N. C. (2016). *Nature and Properties of Soils, The, 15th edition*. Pearson. https://www.pearson.com/en-us/subject-catalog/p/nature-and-properties-of-soils-the/P200000000825/9780137516933

Burgess, D., Baldock, J. A., Wetzell, S., & Brand, D. G. (1995). Scarification, fertilization and herbicide treatment effects on planted conifers and soil fertility. *Plant and Soil*, *168*(1), 513-522. https://doi.org/10.1007/BF00029364

Burghoff, T. (2016). Linear-Mixed Models—A Practical Guide Using Statistical Software, Second Edition. B. T. West, K. B. Welch, and A. T. Galecki. (2015). Boca Raton, FL: Taylor and Francis/CRC Press. 440 pages, ISBN-10: 1466560991, ISBN-13: 978–1466560994. *Biometrical Journal*, *58*(3), 717-718. https://doi.org/https://doi.org/10.1002/bimj.201500240

Butnan, S., & Vityakon, P. (2020). The interactive effects of soil disturbance and residue quality on soil nitrogen mineralisation in a tropical sandy soil. *Soil Research*, *58*(3), 277-288. https://doi.org/10.1071/sr18350

Cassel, D. K., & Nielsen, D. R. (1986). Field Capacity and Available Water Capacity. In *Methods of Soil Analysis* (pp. 901-926). https://doi.org/https://doi.org/10.2136/sssabookser5.1.2ed.c36

Chantigny, M. H. (2003). Dissolved and water-extractable organic matter in soils: a review on the influence of land use and management practices. *Geoderma*, *113*(3), 357-380. https://doi.org/https://doi.org/10.1016/S0016-7061(02)00370-1

Ciais, P., Chris, S., Govindasamy, B., Bopp, L., Brovkin, V., Canadell, J., Chhabra, A., Defries, R., Galloway, J., & Heimann, M. (2013). Carbon and other biogeochemical cycles. *Climate Change 2013: The Physical Science Basis*, 465-570.

Cotrufo, M. F., Ranalli, M. G., Haddix, M. L., Six, J., & Lugato, E. (2019). Soil carbon storage informed by particulate and mineral-associated organic matter. *Nature Geoscience*, *12*(12), 989-994. https://doi.org/10.1038/s41561-019-0484-6

Cotrufo, M. F., Soong, J. L., Horton, A. J., Campbell, E. E., Haddix, Michelle L., Wall, D. H., & Parton, W. J. (2015). Formation of soil organic matter via biochemical and physical pathways of litter mass loss. *Nature Geoscience*, *8*(10), 776-779. https://doi.org/10.1038/ngeo2520

Cotrufo, M. F., Wallenstein, M. D., Boot, C. M., Denef, K., & Paul, E. (2013). The Microbial Efficiency-Matrix Stabilization (MEMS) framework integrates plant litter decomposition with soil organic matter stabilization: do labile plant inputs form stable soil organic matter? *Global Change Biology*, *19*(4), 988-995. https://doi.org/https://doi.org/10.1111/gcb.12113

Craine, J. M., Elmore, A. J., Wang, L., Augusto, L., Baisden, W. T., Brookshire, E. N., Cramer, M. D., Hasselquist, N. J., Hobbie, E. A., Kahmen, A., Koba, K., Kranabetter, J. M., Mack, M. C., Marin-Spiotta, E., Mayor, J. R., McLauchlan,

K. K., Michelsen, A., Nardoto, G. B., Oliveira, R. S., . . . Zeller, B. (2015). Convergence of soil nitrogen isotopes across global climate gradients. *Sci Rep*, *5*, 8280. https://doi.org/10.1038/srep08280

Craine, J. M., Morrow, C., & Fierer, N. (2007). MICROBIAL NITROGEN LIMITATION INCREASES DECOMPOSITION. *Ecology*, *88*(8), 2105-2113. https://doi.org/https://doi.org/10.1890/06-1847.1

Davidson, E. A., & Janssens, I. A. (2006). Temperature sensitivity of soil carbon decomposition and feedbacks to climate change. *Nature*, *440*(7081), 165-173. https://doi.org/10.1038/nature04514

DelSontro, T., Boutet, L., St-Pierre, A., del Giorgio, P. A., & Prairie, Y. T. (2016). Methane ebullition and diffusion from northern ponds and lakes regulated by the interaction between temperature and system productivity. *Limnology and Oceanography*, *61*(S1), S62-S77. https://doi.org/https://doi.org/10.1002/lno.10335

Dhaliwal, G., Gupta, N., Kukal, S., & Kaur, M. (2011). Standardization of Automated Vario EL III CHNS Analyzer for Total Carbon and Nitrogen Determination in Soils. *Communications in Soil Science and Plant Analysis*, *42*, 971-979. https://doi.org/10.1080/00103624.2011.558965

Dufour, B., Hébert, F., & Boucher, J.-F. (2024). Temporal changes in forest floor carbon stocks following scarification in boreal lichen woodlands. *Scandinavian Journal of Forest Research*, *39*(2), 101-109. https://doi.org/10.1080/02827581.2024.2305186

Faubert, P., Ribeiro Paula, R., Bouchard, S., Marty, C., Fradette, O., & Villeneuve, C. (2023). Funding research using climate change mitigation: The case of the Carbone boréal research infrastructure. *PLOS Climate*, *2*(6), e0000232. https://doi.org/10.1371/journal.pclm.0000232

Fierer, N., & Schimel, J. P. (2002). Effects of drying–rewetting frequency on soil carbon and nitrogen transformations. *Soil Biology and Biochemistry*, *34*(6), 777-787. https://doi.org/https://doi.org/10.1016/S0038-0717(02)00007-X

Fontaine, S., Barot, S., Barré, P., Bdioui, N., Mary, B., & Rumpel, C. (2007). Stability of organic carbon in deep soil layers controlled by fresh carbon supply. *Nature*, *450*(7167), 277-280. https://doi.org/10.1038/nature06275

Friedlingstein, P., O'Sullivan, M., Jones, M. W., Andrew, R. M., Bakker, D. C. E., Hauck, J., Landschützer, P., Le Quéré, C., Li, H., Luijkx, I. T., Peters, G. P., Peters, W., Pongratz, J., Schwingshackl, C., Sitch, S., Canadell, J. G., Ciais, P., Aas, K., Alin, S. R., . . . Zeng, J. (2026). Global Carbon Budget 2025. *Earth Syst. Sci. Data*, *18*(5), 3211-3288. https://doi.org/10.5194/essd-18-3211-2026

Gaboury, S., Boucher, J.-F., Villeneuve, C., Lord, D., & Gagnon, R. (2009). Estimating the net carbon balance of boreal open woodland afforestation: A case-study in Québec's closed-crown boreal forest. *Forest Ecology and Management*, *257*, 483-494. https://doi.org/10.1016/j.foreco.2008.09.037

García-Palacios, P., Bradford, M. A., Benavente-Ferraces, I., de Celis, M., Delgado-Baquerizo, M., García-Gil, J. C., Gaitán, J. J., Goñi-Urtiaga, A., Mueller, C. W., Panettieri, M., Rey, A., Sáez-Sandino, T., Schuur, E. A. G., Sokol, N. W., Tedersoo, L., & Plaza, C. (2024). Dominance of particulate organic carbon in

top mineral soils in cold regions. *Nature Geoscience*, *17*(2), 145-150. https://doi.org/10.1038/s41561-023-01354-5

Gelman, A., & Hill, J. (2006). *Data Analysis Using Regression and Multilevel/Hierarchical Models*. Cambridge University Press. https://doi.org/DOI: 10.1017/CBO9780511790942

Girard, F., Payette, S., & Gagnon, R. (2009). Origin of the lichen–spruce woodland in the closed-crown forest zone of eastern Canada. *Global Ecology and Biogeography*, *18*(3), 291-303. https://doi.org/https://doi.org/10.1111/j.1466-8238.2009.00449.x

Gonzalez, E. (2013). Lichen-Spruce Woodland Early Indicators of Ecological Resilience Following Silvicultural Disturbances in Québec's Closed-Crown Forest Zone. *American Journal of Plant Sciences*, *04*, 749-765. https://doi.org/10.4236/ajps.2013.43A094

Hannam, K. D., Quideau, S. A., & Kishchuk, B. E. (2006). Forest floor microbial communities in relation to stand composition and timber harvesting in northern Alberta. *Soil Biology and Biochemistry*, *38*(9), 2565-2575. https://doi.org/https://doi.org/10.1016/j.soilbio.2006.03.015

Hartig, F. (2024). *DHARMa: Residual Diagnostics for Hierarchical (Multi-Level / Mixed) Regression Models*. http://florianhartig.github.io/DHARMa/

Hébert, F., Boucher, J.-F., Bernier, P. Y., & Lord, D. (2006). Growth response and water relations of 3-year-old planted black spruce and jack pine seedlings in site prepared lichen woodlands. *Forest Ecology and Management*, *223*(1), 226-236. https://doi.org/https://doi.org/10.1016/j.foreco.2005.11.005

Högberg, P., Nordgren, A., Buchmann, N., Taylor, A. F. S., Ekblad, A., Högberg, M. N., Nyberg, G., Ottosson-Löfvenius, M., & Read, D. J. (2001). Large-scale forest girdling shows that current photosynthesis drives soil respiration. *Nature*, *411*(6839), 789-792. https://doi.org/10.1038/35081058

Hope, G. D. (2007). Changes in soil properties, tree growth, and nutrition over a period of 10 years after stump removal and scarification on moderately coarse soils in interior British Columbia. *Forest Ecology and Management*, *242*(2), 625-635. https://doi.org/https://doi.org/10.1016/j.foreco.2007.01.072

IPCC. (2022). *(Intergovernmental Panel on Climate Change). Climate Change 2022: Mitigation of Climate Change. Contribution of Working Group III to the Sixth Assessment Report of the Intergovernmental Panel on Climate Change. Cambridge, UK and New York, NY, USA: 2022.*

Jandl, R., Lindner, M., Vesterdal, L., Bauwens, B., Baritz, R., Hagedorn, F., Johnson, D. W., Minkkinen, K., & Byrne, K. A. (2007). How strongly can forest management influence soil carbon sequestration? *Geoderma*, *137*(3), 253-268. https://doi.org/https://doi.org/10.1016/j.geoderma.2006.09.003

Jasinski, J. P., & Payette, S. (2005). The creation of alternative stable states in the southern boreal forest, Qu??bec, Canada. *Ecological Monographs - ECOL MONOGR*, *75*, 561-583. https://doi.org/10.1890/04-1621

Johansson, M. B. (1994). The influence of soil scarification on the turn-over rate of slash needles and nutrient release. *Scandinavian Journal of Forest Research*, *9*(1-4), 170-179. https://doi.org/10.1080/02827589409382828

Jones, D. L., & Willett, V. B. (2006). Experimental evaluation of methods to quantify dissolved organic nitrogen (DON) and dissolved organic carbon (DOC) in soil. *Soil Biology and Biochemistry*, *38*(5), 991-999. https://doi.org/https://doi.org/10.1016/j.soilbio.2005.08.012

Kaiser, K., & Guggenberger, G. (2000). The role of DOM sorption to mineral surfaces in the preservation of organic matter in soils. *Organic Geochemistry*, *31*(7), 711-725. https://doi.org/https://doi.org/10.1016/S0146-6380(00)00046-2

Kalbitz, K., Glaser, B., & Bol, R. (2004). Clear-cutting of a Norway spruce stand: implications for controls on the dynamics of dissolved organic matter in the forest floor. *European Journal of Soil Science*, *55*(2), 401-413. https://doi.org/https://doi.org/10.1111/j.1351-0754.2004.00609.x

Kalbitz, K., Solinger, S., Park, J.-H., Michalzik, B., & Matzner, E. (2000). CONTROLS ON THE DYNAMICS OF DISSOLVED ORGANIC MATTER IN SOILS: A REVIEW. *Soil Science*, *165*(4), 277-304. https://journals.lww.com/soilsci/fulltext/2000/04000/controls_on_the_dynamics_of_dissolved_organic.1.aspx

Kataja-aho, S., Smolander, A., Fritze, H., Norrgård, S., & Haimi, J. (2012). Responses of soil carbon and nitrogen transformations to stump removal. *Silva Fennica*, *46*, 169-179. https://doi.org/10.14214/sf.53

Kaye, J. P., & Hart, S. C. (1997). Competition for nitrogen between plants and soil microorganisms. *Trends in Ecology & Evolution*, *12*(4), 139-143. https://doi.org/10.1016/S0169-5347(97)01001-X

Kennedy, P., Kennedy, H., & Papadimitriou, S. (2005). The effect of acidification on the determination of organic carbon, total nitrogen and their stable isotopic composition in algae and marine sediment. *Rapid Communications in Mass Spectrometry*, *19*(8), 1063-1068. https://doi.org/https://doi.org/10.1002/rcm.1889

Klopp, H. (2024). Carbon to Nitrogen Ratio of Healthy Soils. *South Dakota State University Extension*. https://doi.org/https://extension.sdstate.edu/carbon-nitrogen-ratio-healthy-soils#:~:text=The%20ideal%20C%3AN%20ratio%20for%20soil%20microbes%20is%2024,the%20soil%20C%3AN%20ratio.

Knorr, W., Prentice, I. C., House, J. I., & Holland, E. A. (2005). Long-term sensitivity of soil carbon turnover to warming. *Nature*, *433*(7023), 298-301. https://doi.org/10.1038/nature03226

Kothawala, D. N., Moore, T. R., & Hendershot, W. H. (2009). Soil Properties Controlling the Adsorption of Dissolved Organic Carbon to Mineral Soils. *Soil Science Society of America Journal*, *73*(6), 1831-1842. https://doi.org/https://doi.org/10.2136/sssaj2008.0254

Kull, S. J. M., S. ; Smyth, C. ; Fellows, M. (2019). *Carbon Budget Model of the Canadian Forest Sector (CBM-CFS3): Archive Index Database Table and Parameter Descriptions. Natural Resources Canada, Canadian Forest Service, Northern Forestry Centre, Edmonton, Alberta. 28 p.*

Kurz, W. A., Shaw, C. H., Boisvenue, C., Stinson, G., Metsaranta, J., Leckie, D., Dyk, A., Smyth, C., & Neilson, E. T. (2013). Carbon in Canada's boreal forest — A

synthesis. *Environmental Reviews*, *21*(4), 260-292. https://doi.org/10.1139/er-2013-0041

Kuzyakov, Y. (2010). Priming effects: Interactions between living and dead organic matter. *Soil Biology and Biochemistry*, *42*(9), 1363-1371. https://doi.org/https://doi.org/10.1016/j.soilbio.2010.04.003

Lafleur, B., Paré, D., Fenton, N. J., & Bergeron, Y. (2011). Growth of planted black spruce seedlings following mechanical site preparation in boreal forested peatlands with variable organic layer thickness: 5-year results. *Annals of Forest Science*, *68*(8), 1291-1302. https://doi.org/10.1007/s13595-011-0136-5

Laganière, J., Paré, D., Bergeron, Y., & Chen, H. Y. H. (2012). The effect of boreal forest composition on soil respiration is mediated through variations in soil temperature and C quality. *Soil Biology and Biochemistry*, *53*, 18-27. https://doi.org/https://doi.org/10.1016/j.soilbio.2012.04.024

Lal, R. (2004). Soil Carbon Sequestration Impacts on Global Climate Change and Food Security. *Science*, *304*(5677), 1623-1627. https://doi.org/doi:10.1126/science.1097396

Lal, R. (2005). Forest soils and carbon sequestration. *Forest Ecology and Management*, *220*(1), 242-258. https://doi.org/https://doi.org/10.1016/j.foreco.2005.08.015

Lavallee, J. M., Soong, J. L., & Cotrufo, M. F. (2020). Conceptualizing soil organic matter into particulate and mineral-associated forms to address global change in the 21st century. *Global Change Biology*, *26*(1), 261-273. https://doi.org/https://doi.org/10.1111/gcb.14859

LeBauer, D. S., & Treseder, K. K. (2008). NITROGEN LIMITATION OF NET PRIMARY PRODUCTIVITY IN TERRESTRIAL ECOSYSTEMS IS GLOBALLY DISTRIBUTED. *Ecology*, *89*(2), 371-379. https://doi.org/https://doi.org/10.1890/06-2057.1

Liu, C.-H., Ho, J.-Y., Chu, C.-R., Chang, C.-H., & Chen, H. (2022). A pixel analysis technique and unmanned aircraft system for horizontal displacement in the landslide potential area. *Geoscience Letters*, *9*(1), 17. https://doi.org/10.1186/s40562-022-00229-8

Lloyd, J., & Taylor, J. A. (1994). On the temperature dependence of soil respiration. *Functional Ecology*, *8*, 315-323.

Mäkipää, R., Abramoff, R., Adamczyk, B., Baldy, V., Biryol, C., Bosela, M., Casals, P., Curiel Yuste, J., Dondini, M., Filipek, S., Garcia-Pausas, J., Gros, R., Gömöryová, E., Hashimoto, S., Hassegawa, M., Immonen, P., Laiho, R., Li, H., Li, Q., . . . Lehtonen, A. (2023). How does management affect soil C sequestration and greenhouse gas fluxes in boreal and temperate forests? – A review. *Forest Ecology and Management*, *529*, 120637. https://doi.org/https://doi.org/10.1016/j.foreco.2022.120637

Mallik, A. U., & Hu, D. (1997). Soil respiration following site preparation treatments in boreal mixedwood forest. *Forest Ecology and Management*, *97*(3), 265-275. https://doi.org/https://doi.org/10.1016/S0378-1127(97)00067-4

Mansuy, N., Gauthier, S., & Bergeron, Y. (2013). Afforestation opportunities when stand productivity is driven by a high risk of natural disturbance: a review of

the open lichen woodland in the eastern boreal forest of Canada. *Mitigation and Adaptation Strategies for Global Change*, *18*(2), 245-264. https://doi.org/10.1007/s11027-012-9362-x

Manzoni, S., Taylor, P., Richter, A., Porporato, A., & Ågren, G. I. (2012). Environmental and stoichiometric controls on microbial carbon-use efficiency in soils. *New Phytologist*, *196*(1), 79-91. https://doi.org/https://doi.org/10.1111/j.1469-8137.2012.04225.x

Marty, Piquette J, Morin H, Bussières D, Thiffault N, Houle D, Bradley RL, Simpson MJ, Ouimet R, & MC, P. (2019). Nine years of in situ soil warming and topography impact the temperature sensitivity and basal respiration rate of the forest floor in a Canadian boreal forest. *PLoS One*, *14*(12), e0226909. https://doi.org/10.1371/journal.pone.0226909

Marty, C., Houle, D., Courchesne, F., & Gagnon, C. (2019). Soil C:N ratio is the main driver of soil δ15N in cold and N-limited eastern Canadian forests. *CATENA*, *172*, 285-294. https://doi.org/https://doi.org/10.1016/j.catena.2018.08.029

Marty, C., Houle, D., Gagnon, C., & Duchesne, L. (2011). Isotopic compositions of S, N and C in soils and vegetation of three forest types in Québec, Canada. *Applied Geochemistry*, *26*(12), 2181-2190. https://doi.org/https://doi.org/10.1016/j.apgeochem.2011.08.002

Marty, C., Ouimet, R., Fradette, O., Paré, M., Faubert, P., & Villeneuve, C. (2024). Assessing soil carbon dynamics following mechanical site preparation in boreal lichen woodlands of Québec, Canada. *Forest Ecology and Management*, *553*, 121600. https://doi.org/https://doi.org/10.1016/j.foreco.2023.121600

Mayer, M., Prescott, C. E., Abaker, W. E. A., Augusto, L., Cécillon, L., Ferreira, G. W. D., James, J., Jandl, R., Katzensteiner, K., Laclau, J.-P., Laganière, J., Nouvellon, Y., Paré, D., Stanturf, J. A., Vanguelova, E. I., & Vesterdal, L. (2020). Tamm Review: Influence of forest management activities on soil organic carbon stocks: A knowledge synthesis. *Forest Ecology and Management*, *466*, 118127. https://doi.org/https://doi.org/10.1016/j.foreco.2020.118127

Militino, A. F. (2010). Mixed Effects Models and Extensions in Ecology with R. *Journal of the Royal Statistical Society Series A: Statistics in Society*, *173*(4), 938-939. https://doi.org/10.1111/j.1467-985X.2010.00663_9.x

Moore, T. R., Paré, D., & Boutin, R. (2008). Production of Dissolved Organic Carbon in Canadian Forest Soils. *Ecosystems*, *11*(5), 740-751. https://doi.org/10.1007/s10021-008-9156-x

Mooshammer, M., Wanek, W., Zechmeister-Boltenstern, S., & Richter, A. A. (2014). Stoichiometric imbalances between terrestrial decomposer communities and their resources: mechanisms and implications of microbial adaptations to their resources [Review]. *Frontiers in Microbiology*, *Volume 5 - 2014*. https://doi.org/10.3389/fmicb.2014.00022

Mundim, K. C., Baraldi, S., Machado, H. G., & Vieira, F. M. C. (2020). Temperature coefficient (Q10) and its applications in biological systems: Beyond the Arrhenius theory. *Ecological Modelling*, *431*, 109127. https://doi.org/https://doi.org/10.1016/j.ecolmodel.2020.109127

Munson, A. D., Margolis, H., & Brand, D. G. (1993). INTENSIVE SILVICULTURAL TREATMENT : IMPACTS ON SOIL FERTILITY AND PLANTED CONIFER RESPONSE. *Soil Science Society of America Journal*, *57*, 246-255.

Nilsson, M.-C., & Wardle, D. A. (2005). Understory vegetation as a forest ecosystem driver: evidence from the northern Swedish boreal forest. *Frontiers in Ecology and the Environment*, *3*(8), 421-428. https://doi.org/https://doi.org/10.1890/1540-9295(2005)003[0421:UVAAFE]2.0.CO;2

Nordborg, F., Nilsson, U., & Örlander, G. (2003). Effects of different soil treatments on growth and net nitrogen uptake of newly planted Picea abies (L.) Karst. seedlings. *Forest Ecology and Management*, *180*(1), 571-582. https://doi.org/https://doi.org/10.1016/S0378-1127(02)00650-3

Ogden, F. L., Allen, M. B., Lai, W., Zhu, J., Seo, M., Douglas, C. C., & Talbot, C. A. (2017). The soil moisture velocity equation. *Journal of Advances in Modeling Earth Systems*, *9*(2), 1473-1487. https://doi.org/https://doi.org/10.1002/2017MS000931

Örlander, G., Gemmel, P., & Hunt, J. (1990). Site preparation: a Swedish overview. *FRDA Report (Victoria, B.C.)*(No. 105), vi + 62 pp.

Ouimet, R., Boucher, J.-F., Tremblay, P., & Lord, D. (2018). Comparing soil profiles of adjacent forest stands with contrasting tree densities: lichen woodlands vs. black spruce–feathermoss stands in the continuous boreal forest. *Canadian Journal of Soil Science*, *98*(3), 458-468. https://doi.org/10.1139/cjss-2018-0017

Pan, Y., Birdsey, R. A., Fang, J., Houghton, R., Kauppi, P. E., Kurz, W. A., Phillips, O. L., Shvidenko, A., Lewis, S. L., Canadell, J. G., Ciais, P., Jackson, R. B., Pacala, S. W., McGuire, A. D., Piao, S., Rautiainen, A., Sitch, S., & Hayes, D. (2011). A Large and Persistent Carbon Sink in the World's Forests. *Science*, *333*(6045), 988-993. https://doi.org/doi:10.1126/science.1201609

Paré, M. C., & Bedard-Haughn, A. (2011). Optimum liquid density in separation of the physically uncomplexed organic matter in Arctic soils. *Canadian Journal of Soil Science*, *91*(1), 65-68. https://doi.org/10.4141/cjss10051

Payette, S., Bhiry, N., Delwaide, A., & Simard, M. (2000). Origin of the lichen woodland at its southern range limit in eastern Canada: the catastrophic impact of insect defoliators and fire on the spruce-moss forest. *Canadian Journal of Forest Research*, *30*(2), 288-305. https://doi.org/10.1139/x99-207

Payette, S., & Delwaide, A. (2018). Tamm review: The North-American lichen woodland. *Forest Ecology and Management*, *417*, 167-183. https://doi.org/https://doi.org/10.1016/j.foreco.2018.02.043

PerkinElmer. (2010). Organic Elemental Analysis of Soils – Understanding the Carbon-Nitrogen Ratio. *PerkinElmer publication*. https://doi.org/https://resources.perkinelmer.com/lab-solutions/resources/docs/app_elementalanalysisofsoils.pdf

Piirainen, S., Finér, L., Mannerkoski, H., & Starr, M. (2002). Effects of forest clear-cutting on the carbon and nitrogen fluxes through podzolic soil horizons. *Plant and Soil*, *239*(2), 301-311. https://doi.org/10.1023/A:1015031718162

Poeplau, C., Don, A., Six, J., Kaiser, M., Benbi, D., Chenu, C., Cotrufo, M. F., Derrien, D., Gioacchini, P., Grand, S., Gregorich, E., Griepentrog, M., Gunina, A., Haddix, M., Kuzyakov, Y., Kühnel, A., Macdonald, L. M., Soong, J., Trigalet, S., . . . Nieder, R. (2018). Isolating organic carbon fractions with varying turnover rates in temperate agricultural soils – A comprehensive method comparison. *Soil Biology and Biochemistry*, *125*, 10-26. https://doi.org/https://doi.org/10.1016/j.soilbio.2018.06.025

PPSystems. (2023). *EGM-5 Portable CO2 Gas Analyzer Operation Manual. PP Systems, Amesbury, MA, USA.* https://ppsystems.com/egm-5/

Prescott, C. E. (2010). Litter decomposition: what controls it and how can we alter it to sequester more carbon in forest soils? *Biogeochemistry*, *101*(1), 133-149. https://doi.org/10.1007/s10533-010-9439-0

Prévost, M. (1992). Effets du scarifiage sur les propriétés du sol, la croissance des semis et la compétition : revue des connaissances actuelles et perspectives de recherches au Québec. *Ann. For. Sci.*, *49*(3), 277-296. https://doi.org/10.1051/forest:19920306

Prévost, M. (1997). Effects of scarification on seedbed coverage and natural regeneration after a group seed-tree cutting in a black spruce (Picea mariana) stand. *Forest Ecology and Management*, *94*(1), 219-231. https://doi.org/https://doi.org/10.1016/S0378-1127(96)03955-2

Qualls, R. G., & Haines, B. L. (1992). Biodegradability of Dissolved Organic Matter in Forest Throughfall, Soil Solution, and Stream Water. *Soil Science Society of America Journal*, *56*(2), 578-586. https://doi.org/https://doi.org/10.2136/sssaj1992.03615995005600020038x

Rumpel, C., & Kögel-Knabner, I. (2011). Deep soil organic matter—a key but poorly understood component of terrestrial C cycle. *Plant and Soil*, *338*(1), 143-158. https://doi.org/10.1007/s11104-010-0391-5

San-Emeterio, L. M., Zavala, L. M., Jiménez-Morillo, N. T., Pérez-Ramos, I. M., & González-Pérez, J. A. (2023). Effects of Climate Change on Soil Organic Matter C and H Isotope Composition in a Mediterranean Savannah (Dehesa): An Assessment Using Py-CSIA. *Environmental Science & Technology*, *57*(37), 13851-13862. https://doi.org/10.1021/acs.est.3c01816

Schimel, J. P., & Bennett, J. (2004). NITROGEN MINERALIZATION: CHALLENGES OF A CHANGING PARADIGM. *Ecology*, *85*(3), 591-602. https://doi.org/https://doi.org/10.1890/03-8002

Schimel, J. P., & Weintraub, M. N. (2003). The implications of exoenzyme activity on microbial carbon and nitrogen limitation in soil: a theoretical model. *Soil Biology and Biochemistry*, *35*(4), 549-563. https://doi.org/https://doi.org/10.1016/S0038-0717(03)00015-4

Schindelin, J., Arganda-Carreras, I., Frise, E., Kaynig, V., Longair, M., Pietzsch, T., Preibisch, S., Rueden, C., Saalfeld, S., Schmid, B., Tinevez, J.-Y., White, D. J., Hartenstein, V., Eliceiri, K., Tomancak, P., & Cardona, A. (2012). Fiji: an open-source platform for biological-image analysis. *Nature Methods*, *9*(7), 676-682. https://doi.org/10.1038/nmeth.2019

Schulte-Uebbing, L., & de Vries, W. (2018). Global-scale impacts of nitrogen deposition on tree carbon sequestration in tropical, temperate, and boreal

forests: A meta-analysis. *Global Change Biology*, *24*(2), e416-e431. https://doi.org/https://doi.org/10.1111/gcb.13862
Smolander, A., Kitunen, V., & Mälkönen, E. (2001). Dissolved soil organic nitrogen and carbon in a Norway spruce stand and an adjacent clear-cut. *Biology and Fertility of Soils*, *33*(3), 190-196. https://doi.org/10.1007/s003740000307
Strömgren, M., Boeraeve, M., Ring, E., Hjelm, K., & Högbom, L. (2026). No effect on soil C stock, but increased tree C stock 17 years after site preparation: Results from two hemiboreal field experiments. *Forest Ecology and Management*, *612*, 123745. https://doi.org/https://doi.org/10.1016/j.foreco.2026.123745
Strömgren, M., Mjöfors, K., & Olsson, B. A. (2017). Soil-surface CO2 flux during the first 2 years after stump harvesting and site preparation in 14 Swedish forests. *Scandinavian Journal of Forest Research*, *32*(3), 213-221. https://doi.org/10.1080/02827581.2016.1221993
Sutinen, R., Gustavsson, N., Hänninen, P., Middleton, M., & Räisänen, M. L. (2019). Impact of mechanical site preparation on soil properties at clear-cut Norway spruce sites on mafic rocks of the Lapland Greenstone Belt. *Soil and Tillage Research*, *186*, 52-63. https://doi.org/https://doi.org/10.1016/j.still.2018.10.013
Tang, J., Cheng, H., & Fang, C. (2017). The temperature sensitivity of soil organic carbon decomposition is not related to labile and recalcitrant carbon. *PLoS One*, *12*(11), e0186675. https://doi.org/10.1371/journal.pone.0186675
Team, R. C. (2021). *R: A Language and Environment for Statistical Computing*. R Foundation for Statistical Computing. http://www.R-project.org.
Thiffault, E., Hannam, K. D., Paré, D., Titus, B. D., Hazlett, P. W., Maynard, D. G., & Brais, S. (2011). Effects of forest biomass harvesting on soil productivity in boreal and temperate forests — A review. *Environmental Reviews*, *19*(NA), 278-309. https://doi.org/10.1139/a11-009
Thiffault, N., Chalifour, D., & Bélanger, L. (2013). Enrichment planting of Picea glauca in boreal mixedwoods: can localized site preparation enhance early seedling survival and growth? *New Forests*, *44*(4), 533-546. https://doi.org/10.1007/s11056-012-9361-5
Trumbore, S. E., & Harden, J. W. (1997). Accumulation and turnover of carbon in organic and mineral soils of the BOREAS northern study area. *Journal of Geophysical Research: Atmospheres*, *102*(D24), 28817-28830. https://doi.org/https://doi.org/10.1029/97JD02231
Verardo, D. J., Froelich, P. N., & McIntyre, A. (1990). Determination of organic carbon and nitrogen in marine sediments using the Carlo Erba NA-1500 analyzer. *Deep Sea Research Part A. Oceanographic Research Papers*, *37*(1), 157-165. https://doi.org/https://doi.org/10.1016/0198-0149(90)90034-S
Williamson, R. F., Reay, M., & Sgouridis, F. (2024). Permaculture Management of Arable Soil Increases Soil Microbial Abundance, Nutrients, and Carbon Stocks Compared to Conventional Agriculture. *Agronomy*, *14*(7), 1446. https://www.mdpi.com/2073-4395/14/7/1446

Yang, X., Bao, N., Li, W., Liu, S., Fu, Y., & Mao, Y. (2021). Soil Nutrient Estimation and Mapping in Farmland Based on UAV Imaging Spectrometry. *Sensors (Basel)*, *21*(11). https://doi.org/10.3390/s21113919

Yu, L., Fan, L., Ciais, P., Sitch, S., Fensholt, R., Xiao, X., Yuan, W., Chen, J., Zhang, Y., Wu, X., Qin, Y., Ma, M., Chang, Z., Wang, M., Yan, K., Song, L., & Wigneron, J.-P. (2023). Carbon dynamics of Western North American boreal forests in response to stand-replacing disturbances. *International Journal of Applied Earth Observation and Geoinformation*, *122*, 103410. https://doi.org/https://doi.org/10.1016/j.jag.2023.103410